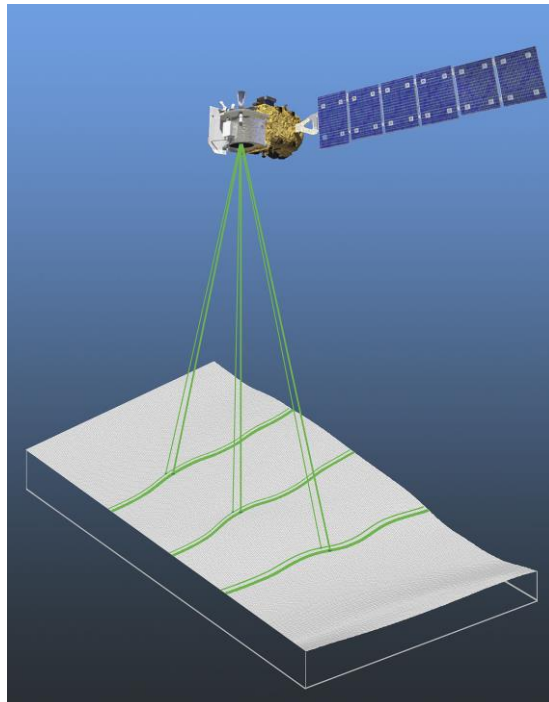


Analysis of river surface slope using ICESat-2 satellite altimetry



Bachelor Thesis
Geodesy & Geoinformatics

University of Stuttgart

Jingyi Bao

Stuttgart, June 2022

Supervisor: Bo Wang, M.Sc

Examiner: Prof. Dr.-Ing. Nico Sneeuw
University of Stuttgart

Erklärung der Urheberschaft

Ich erkläre hiermit an Eides statt, dass ich die vorliegende Arbeit ohne Hilfe Dritter und ohne Benutzung anderer als der angegebenen Hilfsmittel angefertigt habe; die aus fremden Quellen direkt oder indirekt bernommenen Gedanken sind als solche kenntlich gemacht. Die Arbeit wurde bisher in gleicher oder hnlicher Form in keiner anderen Prfungsbehrde vorgelegt und auch noch nicht verffentlicht.

Ort, Datum

Unterschrift

Abstract

Inland surface water bodies (e.g. lakes and rivers) are very important to the nature and human society. To monitor the water level of inland water bodies, gauge stations were built thousand years ago (e.g. nilometer), but the amount of the stations is declining since the 1970s because of lack of maintenance. An accurate and continuous monitoring of lakes and rivers is available with an accuracy of about 1-2 cm for a single measurement because of the satellite altimetry missions launched, e.g. Jason-2 and ENVISAT. These satellites can provide water level with limited spatial and temporal resolution.

In the recent past, researchers have used different satellite mission observations to generate time series of inland water level for monitoring the water bodies. But all those satellites are based on radar altimetry which has its own inconvenience and disadvantages. Those would be discussed in Chapter 2. In 2018 NASA launched a new laser satellite called ICESat-2 to collect laser altimeter data aimed at deriving surface heights of the marine and terrestrial cryosphere, and to observe heights of other Earth surfaces, including land, inland water, ocean, as well as atmospheric layers.

In this thesis the water surface height of two research areas in Yangtze River is calculated and validated. After this the four different types of slopes are calculated:

- Slope of the reach
- Slope between strong and weak beam in one pair
- Slope of the river cross section
- Slope along the river in one beam

After result validations and comparisons it can be seen that the slopes of the river are strongly influenced by seasons. During flooding and non-flooding seasons the slopes can vary a lot. Moreover, the complicated topographies of the river should also be considered. River islands, weirs, dams and other possible elements will influence the water level significantly. The shorter distance is, the more obvious influence those factors could have on slopes, according to the equation $slope = \frac{\Delta h}{d}$ and error propagation. In this project, both slope between strong and weak beam in one pair and slope along the river in one beam are strongly influenced by the local topographies. The differences between the results of the overlapping areas at two epochs could reach 40 cm/km.

Moreover, the slope of the river cross section is decided additionally by both the curvature and the velocity of the river. According to the equation $F_C = m \frac{v^2}{r} = mr\omega^2$, the bigger the curvature and velocity are, the stronger the centrifugal force is. Therefore, the bigger the slope of the river cross section could be.

Contents

Abstract	v
1 Introduction	1
1.1 Motivation	1
1.2 Goals	3
1.3 Structure of this thesis	4
2 ICESat-2 Altimetry	5
2.1 ICESat-2 satellite	5
2.2 ATLAS	6
2.3 Technical specifications	7
2.3.1 Reference Ground Track (RGT)	7
2.3.2 Key ATLAS Performance Specifications	8
2.3.3 ATLAS expected performance	9
2.4 Reference systems used in ICESat-2 Altimetry	9
2.4.1 The relation between orthometric height and ellipsoidal height	10
2.5 Data acquisition and processing	10
2.5.1 ATL03	10
2.5.2 ATL13	11
3 Study area	13
3.1 Study area	13
3.1.1 A mountainous area near Chongqing	13
3.1.2 Downstream of Three Gorges Dam	14
3.2 OpenAltimetry	15
3.3 SWORD	15
3.3.1 Data Formats	16
3.3.2 The used Attribute Description	16
4 Deriving water level from datasets	17
4.1 Intersection calculation	17
4.2 Search radius definition	18

4.3	Outlier rejection	18
4.4	Water level calculation	19
4.5	Special case	19
4.5.1	Lower branch	21
4.5.2	Upper branch	21
5	Different types of slopes	23
5.1	Slope of the reach	23
5.2	Slope between strong and weak beam in one pair	24
5.3	Slope of the river cross section	25
5.3.1	Motivation	25
5.3.2	The relation between curvature and centrifugal force	25
5.4	Slope along the river in one beam	27
6	Results and validations of the first study case	29
6.1	The heights derived from satellite track No.964	29
6.1.1	The validation of the height of each intersection	30
6.1.2	The validation of the height of each middle point	31
6.1.3	Comparison of the heights at two epochs	34
6.2	The heights derived from satellite track No.728	38
6.2.1	The validation of the height of each intersection	39
6.2.2	The validation of the height of each middle point	40
6.2.3	The comparison of the heights at two epochs	42
6.3	Slope of the reach	46
6.3.1	Results derived from satellite track No.964	46
6.3.2	Results derived from satellite track No. 728	48
6.3.3	The comparison of the results between track No.964 and track No.728 in close areas	51
6.4	Slope between strong and weak beam in one pair	52
6.4.1	Results derived from satellite track No.964	52
6.4.2	Results derived from satellite track No.728	54
6.5	Slope along the river in one beam	57
6.5.1	Results derived from satellite track No. 964	57
6.5.2	Results derived from satellite track No.728 on 10.11.2020	58
6.5.3	Results derived from satellite track No.728 on 10.08.2021	59
6.6	Slope of the river cross section	60
6.6.1	Results derived from satellite track No.964 on 31.05.2019	60
6.6.2	Results derived from satellite track No. 964 on 27.08.2020	61
6.6.3	Results derived from satellite track No. 728 on 10.11.2020	62

6.6.4	Results derived from satellite track No. 728 on 10.08.2021 . . .	64
6.6.5	The comparison of the results of track No.728 at two epochs	65
7	Results and validations of downstream of the Three Gorges Dam	67
7.1	Results of the calculated heights	67
7.2	Slope of the reach	69
7.3	Slope of the river cross section	70
7.4	Special case - the satellite ground tracks cross the dam	72
8	Summary and conclusion	75
	References	77

List of Figures

1.1	The first study area	3
1.2	The second study area	3
2.1	The abridged general view of ICESat-2 (credit: NASA)	5
2.2	Example of the space laser[McGarry, 2020]	7
2.3	The abridged general view of ICESat-2's RGT [Zhang et al., 2021]	8
2.4	The difference between orthometric and ellipsoidal heights	10
3.1	The first study reach of Yangtze River	13
3.2	The second study reach of Yangtze River	15
4.1	The chosen principle of intersection point (credit: Google Earth)	17
4.2	The extraction of measurements	18
4.3	The centerline and the satellite ground track ran across the river island	20
4.4	The lower branch of the stream	21
5.1	Scheme of the slope of the reach (credit: Google earth)	23
5.2	Scheme of the slope between strong and weak bean within one pair (credit: Google earth)	24
5.3	Scheme of the methodology of the calculation of cross section slope (credit: Google earth)	26
5.4	A diagram of the projection. credit: Google earth	27
6.1	Track ID 964 at two epochs	29
6.2	Track ID 964 Intersections	30
6.3	A scheme of the projection. credit: Google earth	32
6.4	The Middle point of one pair	32
6.5	The weir near middle point 3	34
6.6	The satellite image on 05.06.2020 (credit: Landsat-8)	35
6.7	The satellite imagery on 29.08.2020 (credit: Landsat-8)	35

6.8	The calculated water levels of 4 different types of points on 31.05.2019 <i>elevation_{strong}</i> : the height of intersection calculated from strong beam <i>elevation_{weak}</i> : the height of intersection calculated from weak beam <i>elevation_{MS}</i> : the height of middle point calculated from strong beam <i>elevation_{MW}</i> : the height of middle point calculated from weak beam	36
6.9	The calculated water levels of 4 different types of points on 27.08.2020 <i>elevation_{strong}</i> : the height of intersection calculated from strong beam <i>elevation_{weak}</i> : the height of intersection calculated from weak beam <i>elevation_{MS}</i> : the height of middle point calculated from strong beam <i>elevation_{MW}</i> : the height of middle point calculated from weak beam	37
6.10	Track ID728 on two epochs	38
6.11	Track ID 728 Intersections	39
6.12	A pair of track (10.11.2020) passed over the weir	40
6.13	Track ID728 Middle points	41
6.14	The satellite image on 12.11.2020 (credit: Landsat-8)	43
6.15	The satellite image on 04.08.2021 (credit: Landsat-8)	43
6.16	The calculated water levels of 4 different types of points on 10.11.2020 <i>elevation_{strong}</i> : the height of intersection calculated from strong beam <i>elevation_{weak}</i> : the height of intersection calculated from weak beam <i>elevation_{MS}</i> : the height of middle point calculated from strong beam <i>elevation_{MW}</i> : the height of middle point calculated from weak beam	44
6.17	The calculated water levels of 4 different types of points on 10.08.2021 <i>elevation_{strong}</i> : the height of intersection calculated from strong beam <i>elevation_{weak}</i> : the height of intersection calculated from weak beam <i>elevation_{MS}</i> : the height of middle point calculated from strong beam <i>elevation_{MW}</i> : the height of middle point calculated from weak beam	45
6.18	The slopes of the reach derived from track ID 964	46
6.19	The slopes of the reach derived from track ID 728 on 10.11.2020	48
6.20	The slopes of the reach derived from track ID 728 on 10.08.2021	49
6.21	The overlapping area of track ID 728 at two epochs	50
6.22	The overlapping areas	51
6.23	The slopes between strong and weak beam in one pair from track ID 964 on 31.05.2019	52
6.24	Track ID964 gt1-3 on 31.05.2019 and on 27.08.2020	53

6.25	The data points of gt3 on 31.05.2019 and on 27.08.2020	53
6.26	The slopes between strong and weak beam in one pair from Track ID728 on 10.11.2020	54
6.27	Track ID728 gt2 on 10.11.2020	55
6.28	Track ID728 gt3-1 on 10.11.2020	55
6.29	The slopes between strong and weak beam in one pair from Track ID728 on 10.08.2021	56
6.30	Track ID 964 strong beams projection	57
6.31	Track ID 728 strong beam projection on 10.11.2020	58
6.32	Track ID 728 strong beam projection on 10.08.2021	59
6.33	The norms of the centerline of the river and the satellite ground tracks on 31.05.2019	60
6.34	The norms of the centerline of the river and the satellite ground tracks on 27.08.2020	61
6.35	The norms of the centerline of the river and the satellite ground tracks on 10.11.2020	62
6.36	The norms of the centerline of the river and the satellite ground tracks on 10.08.2021	64
6.37	Track ID 728 at two epochs	65
7.1	The intersections of Track ID 95 on 04.04.2019	67
7.2	The intersections of Track ID 743 on 11.11.2020	68
7.3	The overlapping area of satellite ground tracks	69
7.4	The norms of the centerline of the river on 04.04.2019	70
7.5	The norms of the centerline of the river on 11.11.2020	71
7.6	Track ID 743 on 15.08.2019	72
7.7	Track ID 743	72

List of Tables

6.1	The results of the heights derived from Track ID 964	30
6.2	The results of the heights on Middle points	33
6.3	The differences of the heights of two epochs	34
6.4	The results of the heights derived from Track ID 728	39
6.5	The results of the heights on Middle points	41
6.6	The differences of the heights at two epochs	42
6.7	The differences of the results at two epochs	46
6.8	The slopes of track ID 728 on 10.11.2020	48
6.9	The results of track ID 728 on 10.08.2021	49
6.10	The comparison of the results of track ID 728 at two epochs	50
6.11	The comparison between track ID 728 and track ID 964	51
6.12	The results of track ID 964 at two epochs	52
6.13	The results of Track ID728 on 10.11.2020	54
6.14	The results of Track ID728 on 10.11.2020	56
6.15	The results of Track ID 964 at two epochs	57
6.16	The results of Track ID 728 on 10.11.2020	58
6.17	The results of Track ID 728 on 10.08.2021	59
6.18	The results of Track ID 964 on 31.05.2019	60
6.19	The results of Track ID 964 on 27.08.2020	61
6.20	The results of Track ID 728 on 10.11.2020	62
6.21	The results of Track ID 728 on 10.08.2021	64
6.22	The results comparison of Track ID 728 at two epochs	66
7.1	The results of orthometric heights derived from Track ID 95	68
7.2	The results of orthometric heights derived from Track ID 743	68
7.3	Slopes of the reach derived from Track ID 95	69
7.4	Slopes of the reach derived from Track ID 743	70
7.5	The results of Track ID 95 on 04.04.2019	70
7.6	The results of Track ID 743 on 11.11.2020	71
7.7	The results of heights derived from Track ID 743	73

Chapter 1

Introduction

1.1 Motivation

Water is one of the most important resources in nature. Water is life. On the earth, the total volume of water is evaluated about $333 \times 10^6 \text{ km}^3$, which includes 97.5 % salt water and 2.5 % fresh water, and 0.3 % of fresh water is in liquid form on the earth surface, i.e. lakes, reservoirs and rivers. The greatest dangers of the coming years are water scarcity and its consequences. Water is essential for life but at the same time water can also be a serious threat, for example when rivers burst their banks, dams break and serious flooding occurs. Climate change will further increase the number and gravity of natural disasters such as water shortages and flooding from heavy rains and storms.

Considering how important water is to human society and in order to face the dangers caused by water scarcity and flooding, it is very imperative to monitor water levels of water bodies and have more effective water management. Moreover, after the data collection of water levels it is possible to calculate the slope. Here slope plays a very important role and works as a key hydraulic variable to determine stream flow.

However here comes a challenge: what happens when IoT (Internet of Things) application needs to be in remote locations? Where no terrestrial connection with cellular networks or internet is available?

Satellite communication is the key solution here! With satellites a global coverage can be achieved. Besides it does not require any power supply and can run with solar power. Compared to the conventional manual in-situ monitoring, global water level monitoring has higher flexibility.

Satellite altimetry-based monitoring of water bodies is an advanced approach. There are in general two different methods: satellite radar altimetry and satellite laser altimetry. Radar altimetry has a relatively poor spatial sampling which is due to its operating principle. This system transmits single radio beam down to the ground and measures the time it takes to be reflected back up to the spacecraft. As we all know, it is impossible to get the information we need to analyze the river slope with only one beam. In order to fix this problem, many studies use the data of multi-mission altimetry, but still have redundant data to process.

With the launch of ICESat-2 laser altimetry in 2018, a higher along-track spatial-resolution sampling is realized compared to radar altimetry. The key advancement of ICESat-2 is that it generates individual footprints of nearly 17 m on the Earth's surface, with each footprint separated by only 70 cm, a much higher resolution than the earlier missions. ATLAS works under the concept of multi-beam approach containing three pairs of strong and weak beams. With the data collected by ICESat-2 the river slope at different locations can be calculated from both strong and weak beams.

In this study, Yangtze River is chosen as the research object. This river plays a critical role in global water bodies. It is the longest river in Asia with the length 6300 km. It is also the seventh-largest river by discharge volume in the world with the average value of 30,146 m³/s. The Three Gorges Dam on the Yangtze River is the largest hydro-electric power station in the world. In recent years, the river has suffered from industrial pollution, plastic pollution, agricultural runoff and loss of wetland and lakes, which exacerbates seasonal flooding. In order to avoid the disastrous consequence of flooding as much as possible, it is important to monitor the water level of Yangtze river and the river slope.

1.2 Goals

In this thesis, we take advantage of ICESat-2 Laser Altimeter data to calculate the river slopes in two different study areas of Yangtze River. The first study area is a mountainous region near Chongqing which means the river slope there is more obvious in comparison to plains. The second area is the Three Gorges Dam where the water level difference before and after the dam can reach 80 m.

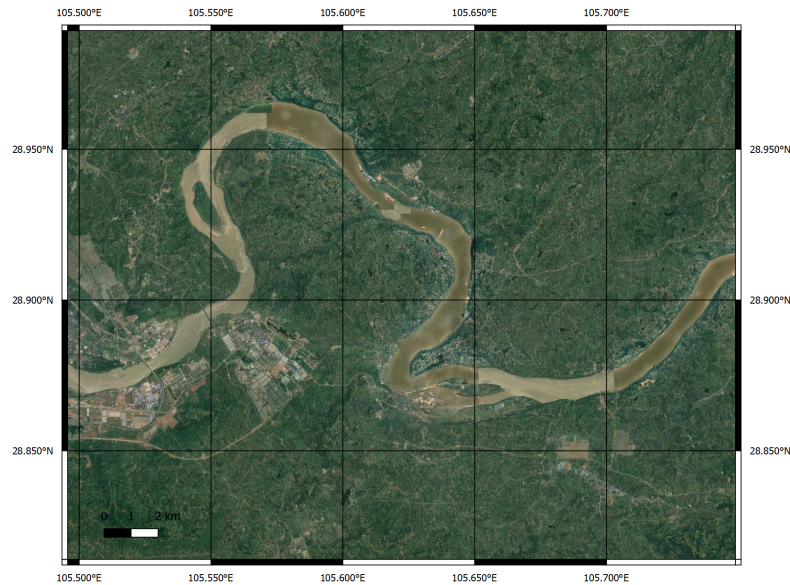


Figure 1.1: The first study area



Figure 1.2: The second study area

The goals in this thesis are shown as follows:

- Deriving the water levels from ICESat-2 database and assessing the quality of the values.
- Calculating four different types of slope.
- Assessing the quality of slope determination.

1.3 Structure of this thesis

The structure of this thesis to implement the objectives is divided into the following chapters. In Chapter 2, the detailed principle of satellite laser altimetry will be presented. Furthermore, ICESat-2 mission and potential challenges will also be introduced in this chapter. In Chapter 3 the two study areas of Yangtze River will be introduced. In Chapter 4 and 5, algorithms of water level calculation and different types of slopes will be explained in more details. For Chapter 6 and 7, we will analyze the results in the two study areas. Chapter 8 indicates the summary and conclusion.

Chapter 2

ICESat-2 Altimetry

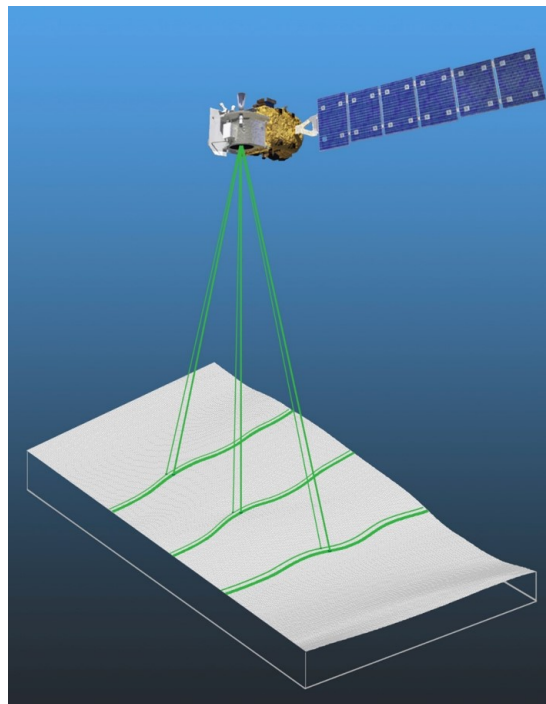


Figure 2.1: The abridged general view of ICESat-2 (credit: NASA)

2.1 ICESat-2 satellite

The ICESat-2 spacecraft provides propulsion, navigation, attitude control, thermal control, data storage and handling, ground communication, and more.

The basic orbital information of ICESat-2 Spacecraft [Jasinski et al., 2021]:

Altitude	498.9 km
Inclination	92°
Repeat	91 nodal days
Speed	6.92 km/s

The spacecraft has a GPS-receiver aboard and a very specific center-of-gravity knowledge so that the satellite could calculate its position. Moreover, ground calibration studies have also been conducted to refine the process even further. Since the mission is that the instrument should measure the distance from itself to the ground, knowing the spacecraft's altitude is the key.

On the ATLAS instrument, along with lasers, telescope and detector, engineers also built in a piece of equipment called the laser reference system. This system controls where the laser is pointing, ensuring that it's aligned with the telescope. The laser reference system also tells the spacecraft where the telescope is pointing just in case any adjustments need to be made.

2.2 ATLAS

ATLAS is the abbreviation for Advanced Topographic Laser Altimeter System. It features technologies that allow it to collect a more detailed, precise picture of the heights of the planet's ice, vegetation, water and so on. ATLAS has three major tasks: Send pulses of laser light to the ground, collect the returning photons in a telescope, and record the photon travel time. The laser light is at 532 nm, a bright green on the visible spectrum. Compared to the laser sending 40 pulses per second on ICESat-1, the laser on ICESat-2 has the frequency of 10,000 Hz.

The pulses of light travel through a series of lenses and mirrors before beaming to the ground. This pathway along the optical bench serves to start the stopwatch on the timing mechanism, check the laser's wavelength, set the size of the ground footprint, ensure that laser and the telescope are perfectly aligned, and split the laser into six beams.

About 20×10^{18} photons leave ATLAS through its box structure with each pulse; only about a dozen return to the satellite's telescope. In order to catch these photons, a beryllium telescope is equipped in ATLAS. ICESat-2's laser beams and telescope need to align exactly to collect measurements. So ATLAS engineers have designed and built the Laser Reference System. This device picks up a fraction of the laser light before it leaves the satellite, and compares the laser positioning to the positioning of the telescope. A steering mechanism then moves the laser beam, if needed. Moreover, a filter is also used to only let through light that is at precisely 532 nm so that the sunlight which naturally reflects off Earth will

not swamp the detectors. One data point is not sufficient to determine elevation. ATLAS picks up a significant amount of background photons: sunlight in the 532 nm range can set off ATLAS's photon detectors, and particulate matter and clouds in the air could skew ground data. So computer programs need to create 'cloud' graphs, showing thousands of data points returned by the instruments.

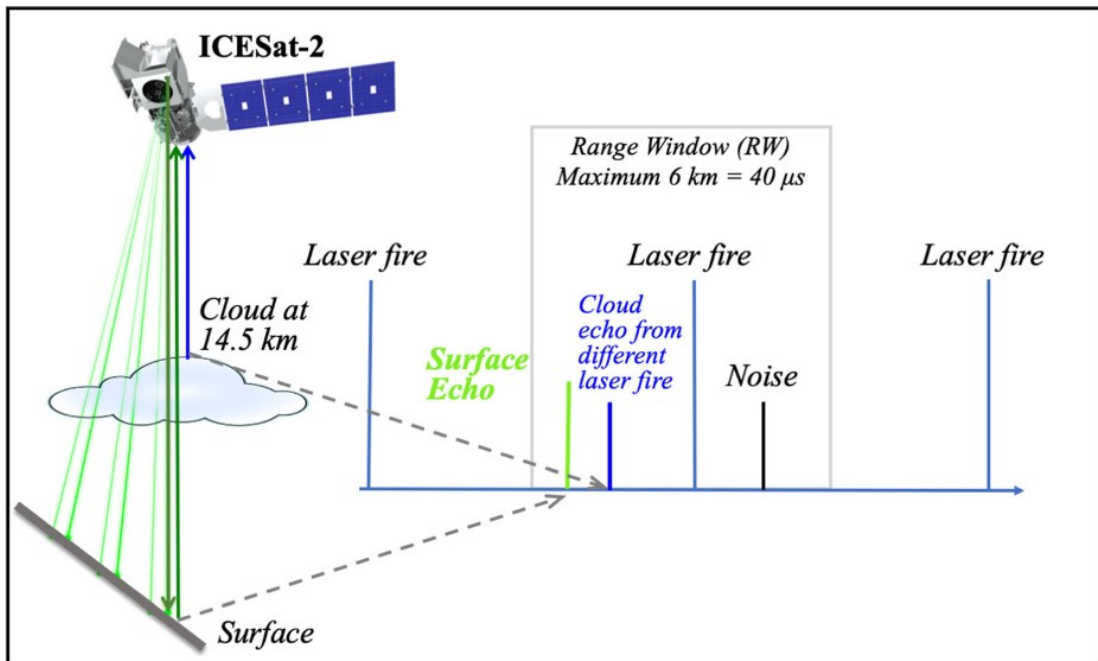


Figure 2.2: Example of the space laser [McGarry, 2020]

2.3 Technical specifications

2.3.1 Reference Ground Track (RGT)

ICESat-2 has in reality 6 tracks per orbit. But in files there are seven tracks: one for each of the six beams of ICESat-2, and the seventh for the Reference Ground Track (RGT). The RGT is actually an imaginary line through the six-beam pattern which is useful for getting a sense of where the orbits fall on Earth. However, the six tracks for the six beams are actually the best estimate of where the beam will fall on Earth's surface.

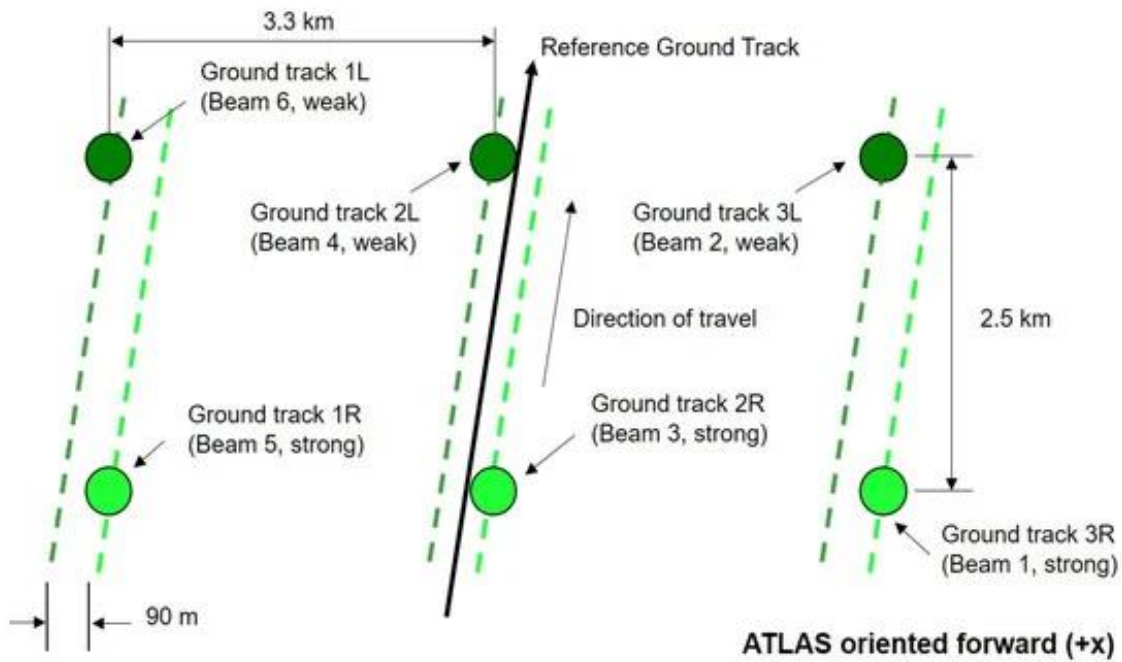


Figure 2.3: The abridged general view of ICESat-2's RGT [Zhang et al., 2021]

2.3.2 Key ATLAS Performance Specifications

For detailed information about ICESat-2 and ATLAS specifications, please see [Neumann et al., 2019].

Nominal duration of mission	3 years
Number of beams	6, organized in 3 pairs
Footprint size	13 m
Field of view	45 m
Pulse repetition frequency	10 kHz(0.7 m on the ground)
Laser wavelength	532 nm
Pointing control	45 m
Pointing knowledge	6.5 m

2.3.3 ATLAS expected performance

Target type	Lambertian surface reflectance (532 nm)	N signal photons per shot (weak beam)	N signal photons per shot (strong beam)	100-shot std dev (weak beam)	100-shot std dev (strong beam)
Ice sheet (interior)	0.9-0.98	0.4-3.0	1.6-12.0	4-9	2-4
Ice sheet (glaciers)	0.6-0.9	0.6-1.0	0.6-3.9	12-29	6-14
Sea Ice	0.8-0.9	0.6-2.1	2.3-8.5	5-8	3-4
Leads	*-0.2	0.05-0.2	0.2-1.0	2-5	2-5

From the above table it is necessary to have strong and weak beam pairs in order to determine the target type. Different types have different performances in range.

2.4 Reference systems used in ICESat-2 Altimetry

Latitudes and longitudes refer to the WGS84 coordinate system. Water surface heights are provided as heights above the WGS84 ellipsoid. The table below provides the basic information of WGS 84:

Geographic coordination system	WGS 84
Projected coordinate system	N/A
Longitude of true origin	Prime Meridian, Greenwich
Latitude of true origin	N/A
Datum	World Geodetic System 1984
Geoid	EGM2008
Units	degrees
Reference	https://epsg.io/4326 (WGS 84)

Moreover, in this project geoid information is needed to convert ellipsoid heights to orthometric heights when in some areas the ATL 13 data is not available or

useful. Geoid reference in the World Geodetic System is EGM. EGM is the abbreviation for the Earth Gravitational Model. The models are provided in two formats: as the series of numerical coefficients to the spherical harmonics which define the model, or a dataset giving the geoid height at each coordinate at a given resolution.

2.4.1 The relation between orthometric height and ellipsoidal height

In this project ATL13 provides orthometric heights while ATL03 provides the ellipsoidal heights. In order to convert the ellipsoidal heights to the orthometric heights the relation as following is needed:

$$h = H + N$$

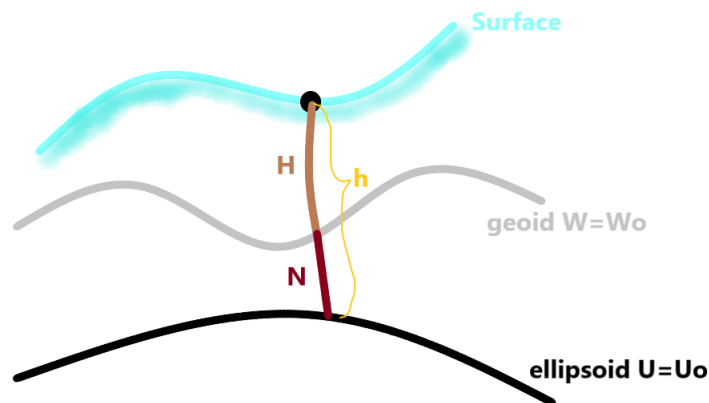


Figure 2.4: The difference between orthometric and ellipsoidal heights

2.5 Data acquisition and processing

2.5.1 ATL03

ATL03 provides global geolocated photon data. It includes precise latitude, longitude and elevation for every received photon, arranged by beam in the along-track direction. Photons classified by signal vs. background, as well as by surface type (land ice, sea ice, land, ocean), including all geophysical corrections (e.g. Earth tides, atmospheric delay, etc...).

2.5.2 ATL13

The ATL13 product is derived from ATL03 product. It provides specifically observations of inland water surface height and exhibits a great potential for monitoring global lake/reservoir water level changes benefiting from its global coverage.

This data set contains along-track water surface heights and descriptive statistics for inland water bodies. Water bodies include lakes, reservoirs, bays, and estuaries. Descriptive statistics include along-track surface slope (where data permit), mean and standard deviation, subsurface signal (532 nm) attenuation, wave height, and coarse depth to bottom topography.

Chapter 3

Study area

In this thesis, ICESat-2 data and Google Earth are used for the aims of this research. These data are available from the websites of their operators, which are free to the public. The Yangtze River in China is selected for the research.

3.1 Study area

3.1.1 A mountainous area near Chongqing

In this study one reach of Yangtze River is extracted with coordinates of N 28°58'25" E 105°40'03", N 28°58'22" E 105°32'47", N 28°51'20" E 105°32'37" and N 28°51'18" E 105°40'12".

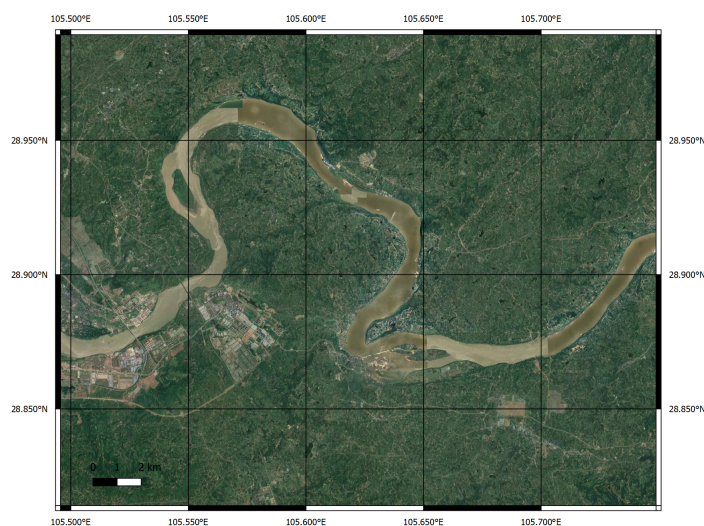


Figure 3.1: The first study reach of Yangtze River

This reach is a mountainous area which means the river slope derived from the data of ICESat-2 is more obvious in comparison to plains. According to the previous research based on the data of the Amazon River whose upper part is consisted of the river systems and flood plains and lower part is located in Amazon basin there is nearly no slope. So it is difficult to observe the slope changes of Amazon River. This is also the reason why I chose this reach.

3.1.2 Downstream of Three Gorges Dam

The approximate position coordinates of the second reach are:

Upstream of the Three Gorges Dam area	
N 30.88° E 110.96°	N 30.81° E 110.96°
N 30.81° E 111.06°	N 30.88° E 111.06°

Downstream of the Three Gorges Dam area	
N 30.86° E 111.11°	N 30.82° E 111.11°
N 30.82° E 111.02°	N 30.86° E 111.03°

The Three Gorges Dam is a hydroelectric gravity dam that spans the Yangtze River by the area of central China. The Three Gorges Dam has been the world's largest power station in terms of installed capacity (22,500 MW) since 2012 [Cleveland, 2013]. As well as producing electricity, the dam is intended to increase the Yangtze River's shipping capacity. By providing flood storage space, the dam reduces the potential for floods downstream which have historically plagued the Yangtze Plain. Thus the Three Gorges Dam project is really important and is a monumental social and economical success.



Figure 3.2: The second study reach of Yangtze River

3.2 OpenAltimetry

OpenAltimetry is a NASA funded collaborative project between the Scripps Institution of Oceanography, San Diego Supercomputer Center, National Snow and Ice Data Center and UNAVCO. OpenAltimetry is a cyberinfrastructure platform (<https://openaltimetry.org/>) for discovery, access, and visualization of data from NASA's ICESat and ICESat-2 missions. These laser profiling altimeters are being used to measure changes in the topography of Earth's ice sheets, vegetation canopy structure, and clouds and aerosols. The unique data from these missions require a new paradigm for data access, to serve the needs of a diverse scientific community and to increase the accessibility and utility of these data for new users.

3.3 SWORD

SWORD is the abbreviation for SWOT (Surface Water and Ocean Topography) River Database. This Database provides a range of relevant data products. One product the SWOT mission will provide are river vector products stored in shape-file format for each SWOT overpass. This type of vector products will be very useful in this research project because they allow multitemporal analysis of river nodes and reaches covering the same river areas. With the help of those products ICESat-2 datasets on different days could be applied to the same river areas by using the same nodes and reaches information.

3.3.1 Data Formats

The SWORD database is provided in netCDF and shapefile formats. All files start with a two-digit continent identifier (“af” – Africa, “as” – Asia / Siberia, “eu” – Europe / Middle East, “na” – North America, “oc” – Oceania, “sa” – South America). File syntax denotes the regional information for each file and varies slightly between netCDF and shapefile formats.

NetCDF files are structured in 3 groups: centerlines, nodes and reaches. The centerline group contains location information and associated reach and node ids along the original GRWL 30m centerlines [Allen and Pavelsky, 2018]. Node and reach groups contain hydrologic attributes at the 200 m node and 10 km reach locations. NetCDFs are distributed at continental scales with a filename convention as follows: [continent]_sword_v1.nc (i.e. na_sword_v1.nc).

3.3.2 The used Attribute Description

- x: Longitude of the node or reach ranging from 180°E to 180°W.
- y: Latitude of the node or reach ranging from 90°S to 90°N.
- node id: ID of each node. The format of the id is as follows: CBBBBBR-RRRNNT where C = Continent (the first number of the Pfafstetter basin code), B = Remaining Pfafstetter basin code up to level 6, R = Reach number (assigned sequentially within a level 6 basin starting at the downstream end working upstream), N = Node number (assigned sequentially within a reach starting at the downstream end working upstream), T = Type (1 – river, 2 – lake off river, 3 – lake on river, 4 – dam or waterfall, 5 – unreliable topology, 6 – ghost node).

Chapter 4

Deriving water level from datasets

4.1 Intersection calculation

A intersection point is defined when a satellite ground track intersects with the centerline of the river. The information of the centerline of Yangtze River could be derived from SWORD. Each time the satellite passes over the water body, the tracks of different sampling dates will not be at the same position. Therefore, the positions of the intersections point will be different on each sampling date.

In this step, it is also necessary to convert the geodetic coordinates into the UTM coordinates and vice versa in order to prepare for the after calculation.

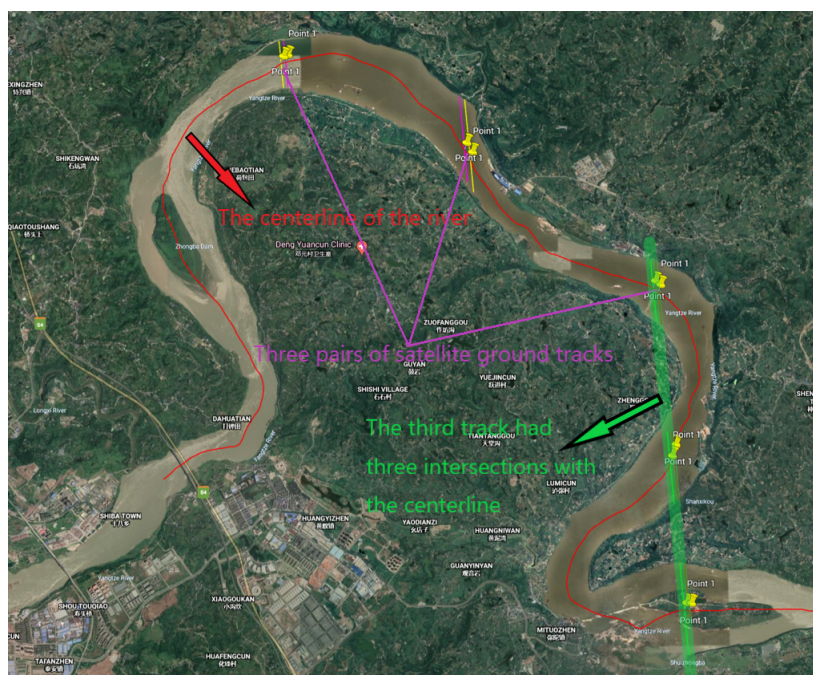


Figure 4.1: The chosen principle of intersection point (credit: Google Earth)

4.2 Search radius definition

Different parts of the river have different width which should be taken into consideration when choosing the search radius. Moreover, strong and weak beams of the satellite ground tracks have different data point densities. Therefore, it is important to define an appropriate search radius so that the proper amount of measurements within this area could be extracted.

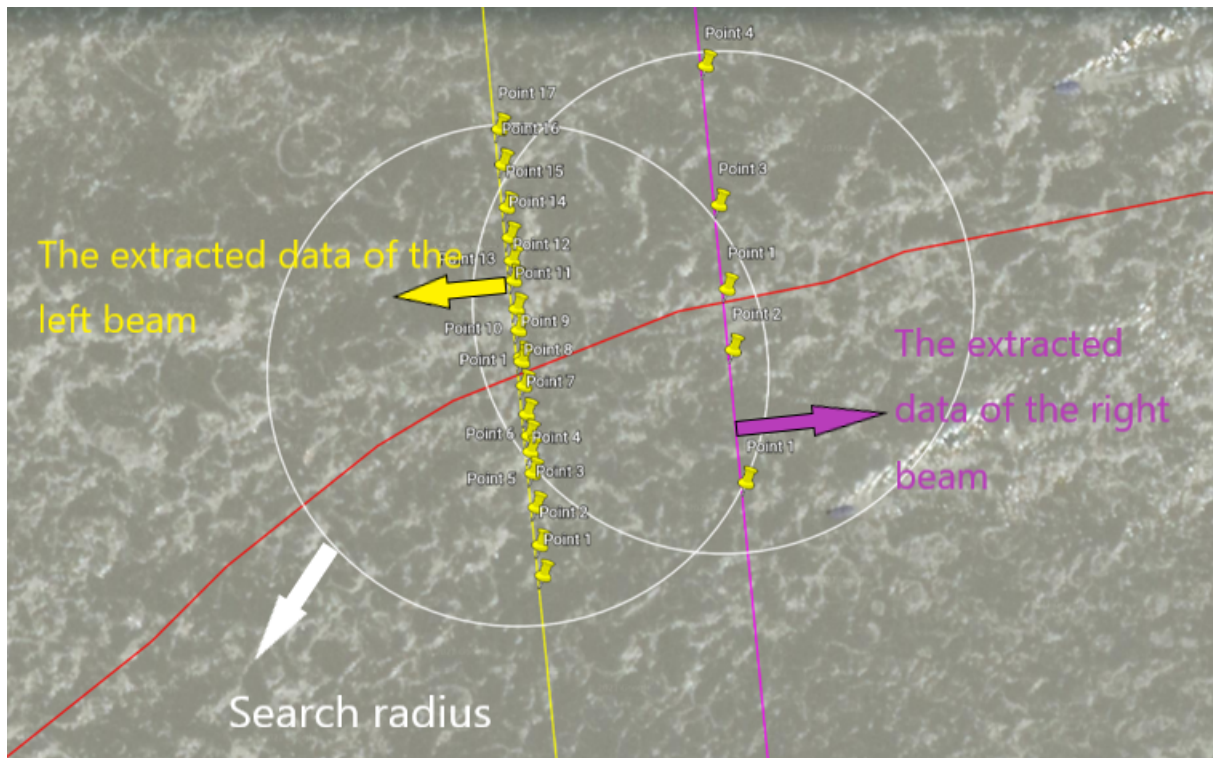


Figure 4.2: The extraction of measurements

4.3 Outlier rejection

In the idealized condition, the calculated water level from each single measurement should be the same in such a small area. However, in reality, outliers may occur sometimes. To improve the accuracy, we use median absolute deviation (MAD) to define a range to exclude outliers.

$$\tilde{X} = \text{median}(X) \quad (4.1)$$

$$\text{MAD} = \text{median}(|X_i - \tilde{X}|) \quad (4.2)$$

$$\tilde{X} - \mu\text{MAD} < X_{\text{extracted}} < \tilde{X} + \mu\text{MAD} \quad (4.3)$$

$$\tilde{X}_{\text{new}} = \text{median}(X_{\text{extracted}}) \quad (4.4)$$

- X : the extracted values of the data sets
- \tilde{X} : the median value of X
- MAD: median absolute deviation
- μ : the common values are 0.5, 1, 1.5, 2
- $X_{\text{extracted}}$: the newly extracted data after outlier rejection

4.4 Water level calculation

After the rejection of the outliers, the median value of the extracted measurements is calculated instead of the mean value to obtain the water level at each intersection point. This is because mean value is easily affected by edge values.

4.5 Special case

In reality there might be an unexpected case, which is a river island. In this case the satellite tracks and the centerline of Yangtze River pass across a river island and the obtained intersection points locate on the island, which means the measured orthometric heights represent actually the river island points' heights. In order to analysis this special case, the algorithms have to be adjusted slightly.

In the example below, the area forks into two branches- the upper branch and the lower branch. In upper branch there are available data points for the required orthometric heights, however, in lower branch somehow there are no ATL13 data points. So each branch requires separate methods to calculate the orthometric heights.

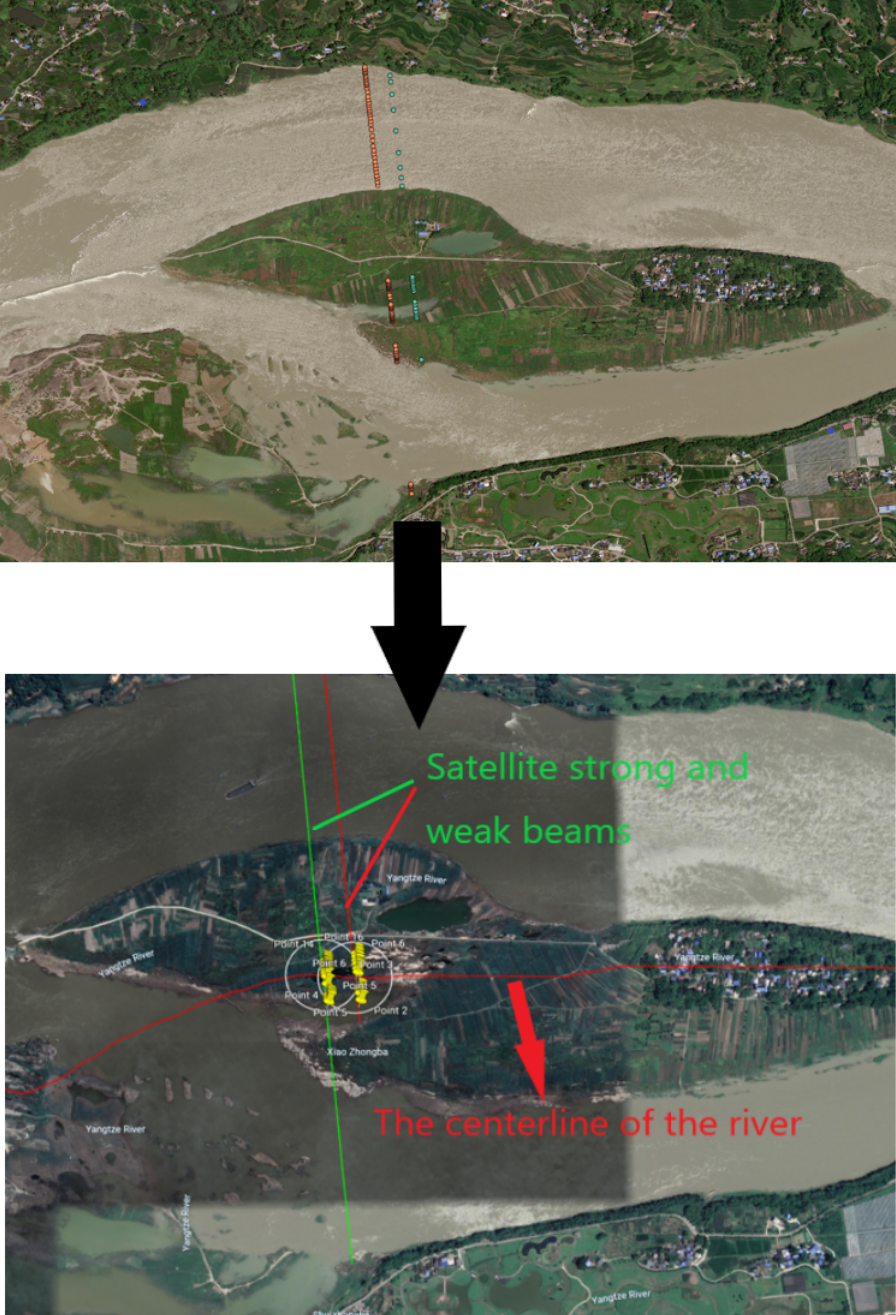


Figure 4.3: The centerline and the satellite ground track ran across the river island



Figure 4.4: The lower branch of the stream

4.5.1 Lower branch

From the above graph it can be seen that there is no data point in the lower branch in this case. Therefore, ATL03 data points will be used instead. Compared to ATL13 which returns the orthometric height, ATL03 returns ellipsoidal height. The relation and conversion between orthometric height and ellipsoidal height has already been discussed in Chapter 2.

4.5.2 Upper branch



From figures above the orthometric heights from strong and weak beams can be derived separately. For each beam the data file of the elevation would be downloaded and repeat the previously mentioned steps to calculate the water level.

Chapter 5

Different types of slopes

5.1 Slope of the reach

In this project, one reach is defined by the centerline of the river between two neighbour strong beams. The requisite formula is below:

$$S = \frac{(h_{C_{i+1}} - h_{C_i})}{l_{C_i-C_{i+1}}} \quad (5.1)$$

h_{C_i} is the water level at the intersection point C_i

$l_{C_i-C_{i+1}}$ is the length between C_i and C_{i+1} along the centerline of the river

i is the index of the intersection

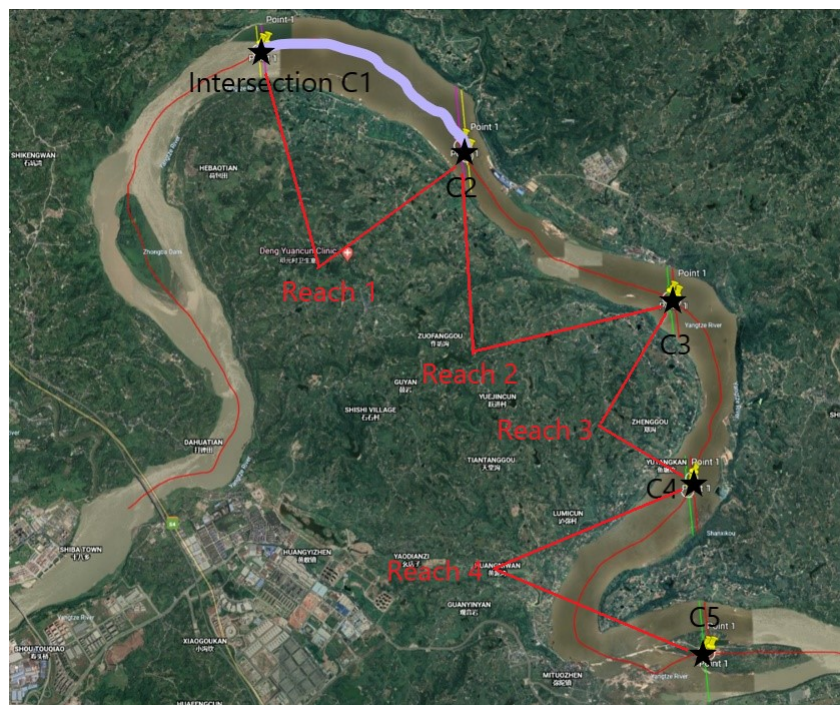


Figure 5.1: Scheme of the slope of the reach (credit: Google earth)

5.2 Slope between strong and weak beam in one pair

Comparing to the slope of the reach, there also exists a height difference between the strong and the weak beams within one pair. The needed formula is below:

$$S = \frac{(h_{\text{cright}} - h_{\text{cleft}})}{l_{\text{left-right}}} \quad (5.2)$$

In which, h_{cleft} is the water level at the intersection point between satellite left ground track and the centerline of the river. $l_{\text{left-right}}$ is the distance between the left and right intersection points within one pair.

Moreover, the distance between the strong and the weak beams within one pair is 90m only when the satellite ground track is perpendicular to the centerline of the river. However, usually the angle between the ground track and the centerline is not exactly 90° which means the distance will be longer than 90m because of the inclination. The more inclined the track is, the longer the distance could be.

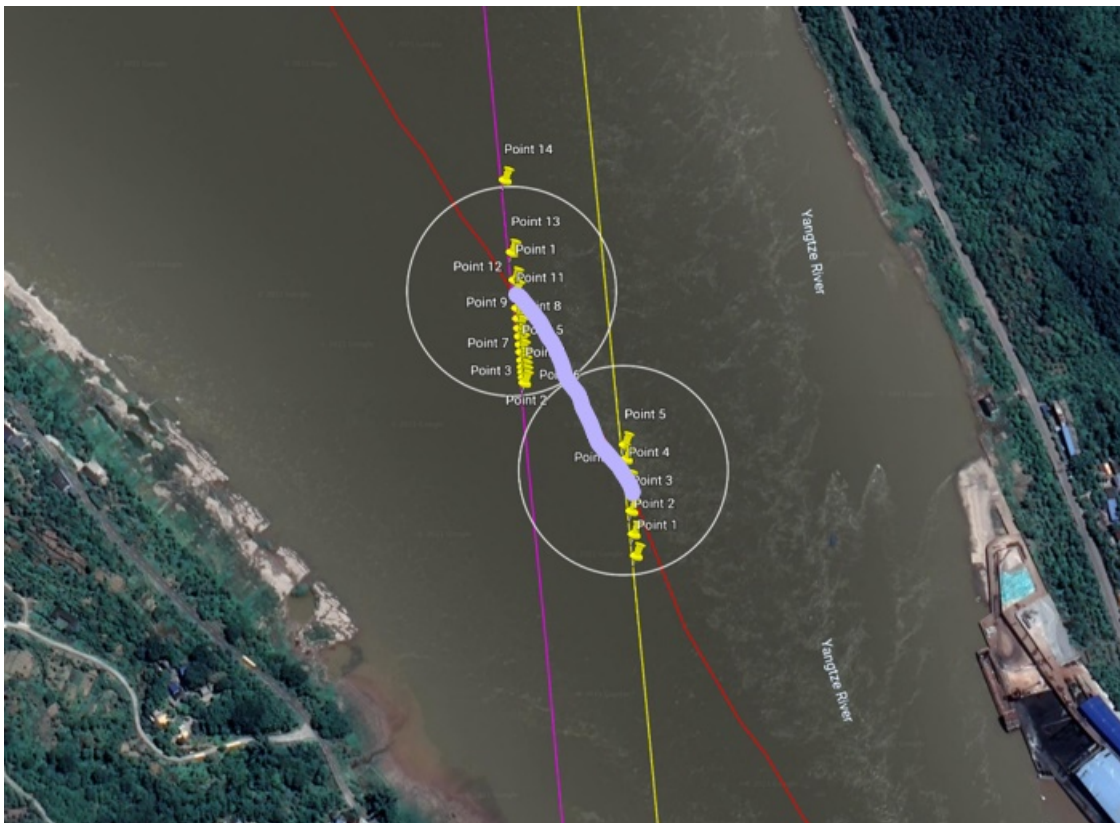


Figure 5.2: Scheme of the slope between strong and weak beam within one pair (credit: Google earth)

5.3 Slope of the river cross section

This type of the slope defines a slope calculated from single strong beam across the river. According to the previous assumption the cross section slope will be more obvious round the bend in the river.

5.3.1 Motivation

Centrifugal force plays an important role in the research about the bend-flow includes velocity and the distribution of the flow. Moreover, centrifugal force also influences the slope of the river cross section. Especially in a river bend the water surface is inclined by the centrifugal force towards the transverse section.

5.3.2 The relation between curvature and centrifugal force

For the centrifugal force there are two expressions in terms of mass, velocity, angular velocity and radius of curvature.

$$F_C = m \frac{v^2}{r} = mr\omega^2 \quad (5.3)$$

Both expressions for centrifugal force can be used. Moreover, centrifugal force is always perpendicular to the curve and pointing to the center of the curvature. This implies that for a given mass and velocity, a large centrifugal force causes a small radius of curvature- that is a tight curve. This also means at the river section which has a greater degree of bend the centrifugal force will be bigger.

Therefore, in order to present the relation between the curvature of the river and the centrifugal force the slope of the river cross section is calculated.

Firstly, build a line perpendicular to the centerline of the river at the intersection point between the satellite ground track and the centerline of the river. Then calculate the shortest distance from each satellite track data point to the obtained vertical line and build the projection.

Secondly, all the data after projection to the vertical line are selected and with the help of data processing Median Absolute Deviation (MAD) the outliers would be excluded.

Thirdly, calculate the orthometric height at the start point of the projected line and the height at the end point and the distance l . Then we use the *fit* function from MATLAB to find the slope of the best fit line, which represents the slope of the cross section.

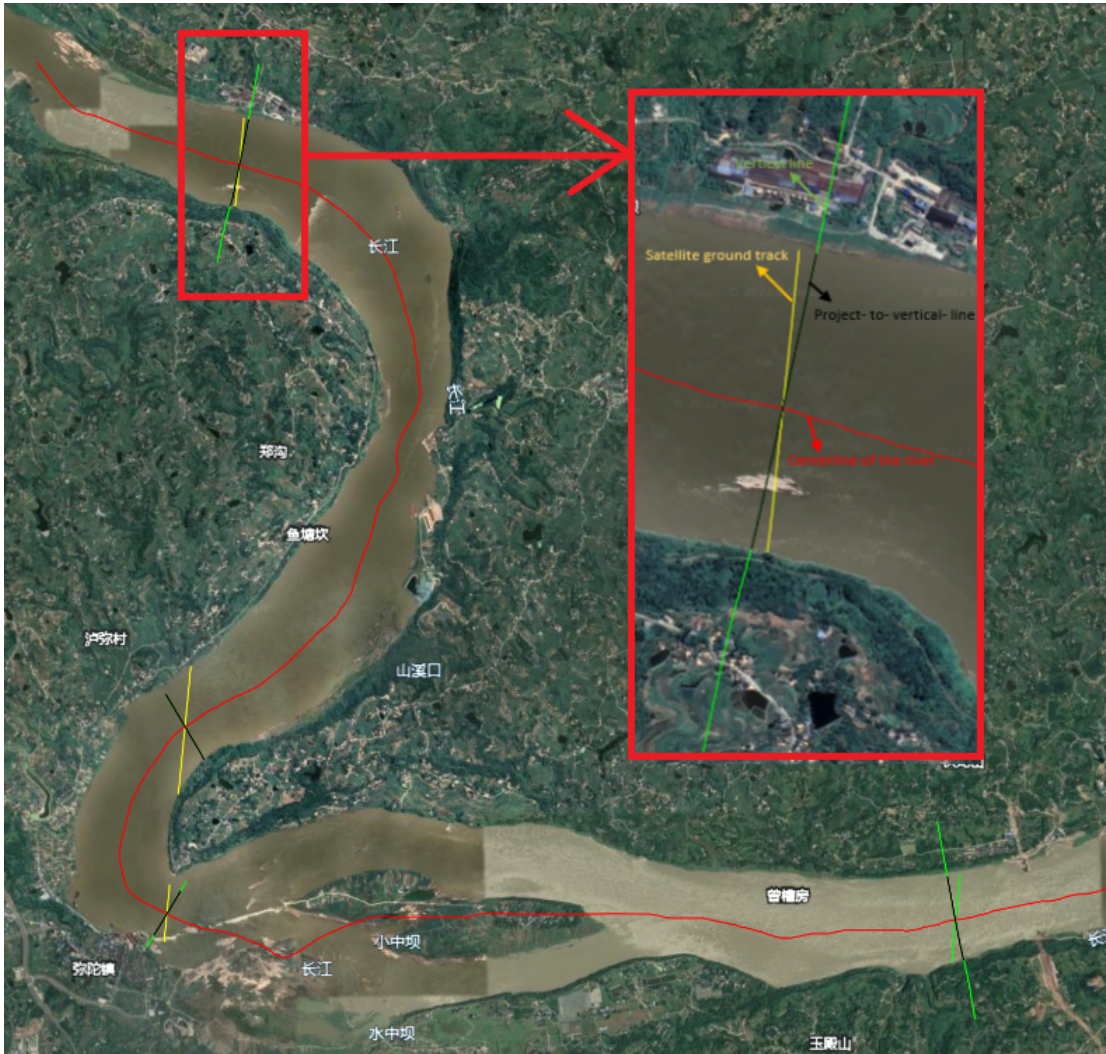


Figure 5.3: Scheme of the methodology of the calculation of cross section slope (credit: Google earth)

5.4 Slope along the river in one beam

This type of the slope is described as the slope of local reach where the track intersects with the river.

Firstly, calculate the angle between the beam and the centerline of the river. If the angle is bigger than 60° , which shows that the beam is close to be perpendicular to the centerline of the river. Then there is no need to calculate the slope, because the water surface height along the track could be assumed a constant across the river.

$$\vec{a} \times \vec{b} = \|\vec{a}\| \|\vec{b}\| \sin\theta \quad (5.4)$$

$$\vec{a} \cdot \vec{b} = \|\vec{a}\| \|\vec{b}\| \cos\theta \quad (5.5)$$

$$\theta = \tan^{-1}\left(\frac{\vec{a} \times \vec{b}}{\vec{a} \cdot \vec{b}}\right) \quad (5.6)$$

Secondly, calculate the shortest distance from each satellite track data to the centerline of the river and build the projection.

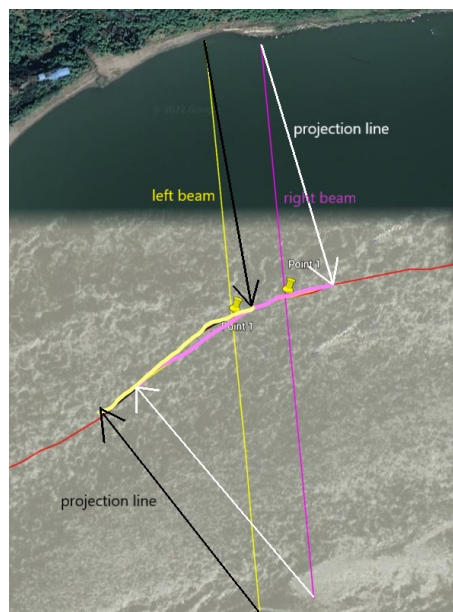


Figure 5.4: A diagram of the projection. credit: Google earth

Thirdly, use *best fit* function to calculate the slope along the river in one beam.

Chapter 6

Results and validations of the first study case

6.1 The heights derived from satellite track No.964



Figure 6.1: Track ID 964 at two epochs

From Figure 6.1, the track ID 964 has available data of research area on 31.05.2019 and 27.08.2020, and the three pairs of beams of each date nearly overlapped.



Figure 6.2: Track ID 964 Intersections

6.1.1 The validation of the height of each intersection

Table 6.1: The results of the heights derived from Track ID 964

05.31.2019	C1	C2	C3	C4	C5	RMSE
Strong beam (m)	219.30	217.90	217.94	215.78	214.12	
Weak beam (m)	219.33	217.88	217.91	215.82	214.17	
Diff (cm)	-3	2	3	-4	-5	3.2
27.08.2020	C1	C2	C3	C4	C5	RMSE
Strong beam (m)	223.61	222.12	222.03	220.64	219.61	
Weak beam (m)	223.63	222.09	222.03	220.67	219.60	
Diff (cm)	-2	3	0	-3	1	2.1

From Table 6.1 there exists the height difference between strong and weak beams for each intersection. The reasons might be as follow:

Firstly, this study area is a mountainous place, originally there is slope between strong and weak beams. As the result, the heights derived from strong and weak beams would not be exactly the same.

Secondly, the distance between strong and weak beams within one pair is not constant. Only when the satellite ground tracks are perpendicular to the centerline of the river, the distance in between is 90 m. Even under the assumption that the slope is a constant, the longer the distance is, the bigger the height difference will be.

Thirdly, the differences are not always positive values. However, all those differences do not exceed the altimetry measurement error range. So the positive and negative differences are acceptable.

6.1.2 The validation of the height of each middle point

In order to reduce the influence caused by distance, the satellite ground tracks will be projected onto the centerline of the river and instead of calculating the water level on both intersection points within one pair, the height on the middle point which is the middle of left and right intersection points will be calculated.

Firstly, the distances from the satellite ground track data points to the centerline of the river will be calculated. For each data point, a minimum distance value and the corresponding centerline node point will be found out. Then a projection of the data points would be built to the river's centerline.

Secondly, calculate the coordinates of the middle point of the left and right intersection points.

$$(X, Y)_{\text{middle}} = \frac{(X_1, Y_1)_{\text{left}} + (X_2, Y_2)_{\text{right}}}{2} \quad (6.1)$$

Thirdly, for the strong beam, define the search radius centered on the middle point and extract the projected points within the range. However, for the weak beam, the measurement of projected point which is closest to the middle point will be directly used, because the available measurements close to the middle point are too few.

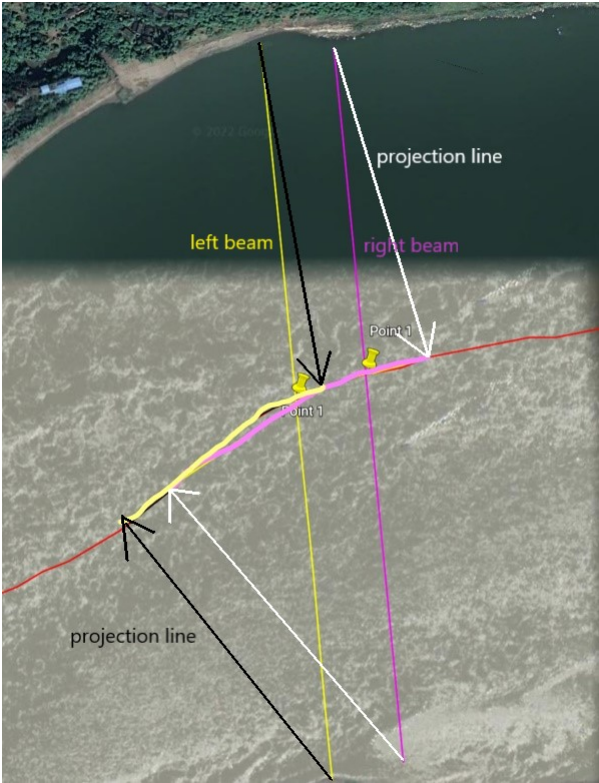


Figure 6.3: A scheme of the projection. credit: Google earth

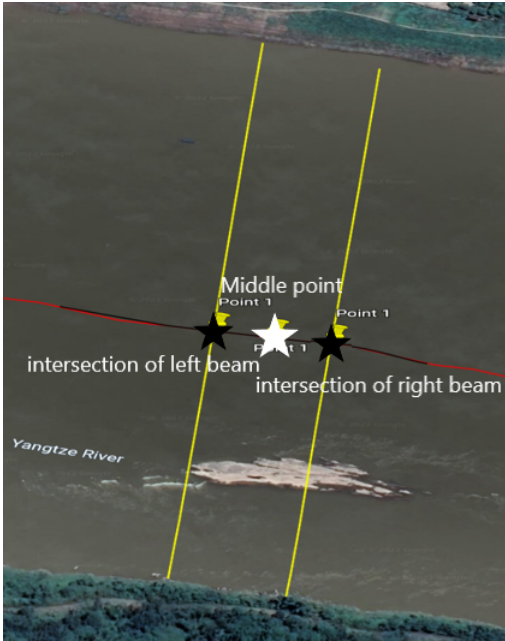


Figure 6.4: The Middle point of one pair

Table 6.2: The results of the heights on Middle points

05.31.2019	Middle1	Middle2	Middle3	Middle5	RMSE
Strong beam (m)	219.30	217.89	217.94	214.11	
Weak beam (m)	219.33	217.90	217.91	214.14	
Diff (cm)	-3	-1	3	-3	2.4
27.08.2020	Middle1	Middle2	Middle3	Middle5	RMSE
Strong beam (m)	223.60	222.08	221.84	219.62	
Weak beam (m)	223.61	222.11	222.12	219.61	
Diff (cm)	-1	-3	-28	1	14.0

From Table 6.2 a conclusion could be obtained that according to RMSE the difference between the heights of middle points from strong and weak beams are not always smaller. By the previous hypothesis, this method should decrease the influence caused by the distance between strong and weak beams, thus, the derived RMSE should be smaller rather than bigger. However, on 27.08.2020 the RMSE is 14.0 cm which is much bigger and abnormal. This unexpected result is mainly resulted from the difference between strong and weak beams on middle point 3. The difference value -28 cm on this point is obviously abnormal. The reason might be as follows:

Firstly, this abnormal difference might be resulted from the limited number of available data points of the weak beam on that day. Due to the too few available weak beam's data points in this case, the value of the closest to middle point data point is regarded as the height instead of defining a search area and calculating the median value. As we know, one measurement is accidental, therefore, using one measurement to represent the calculated value might be very inaccurate.

Secondly, from Figure 6.5 there exists a weir around the middle point 3. The weir has the function of adjusting the stream so this might influence the water level and lead to the abnormal difference.

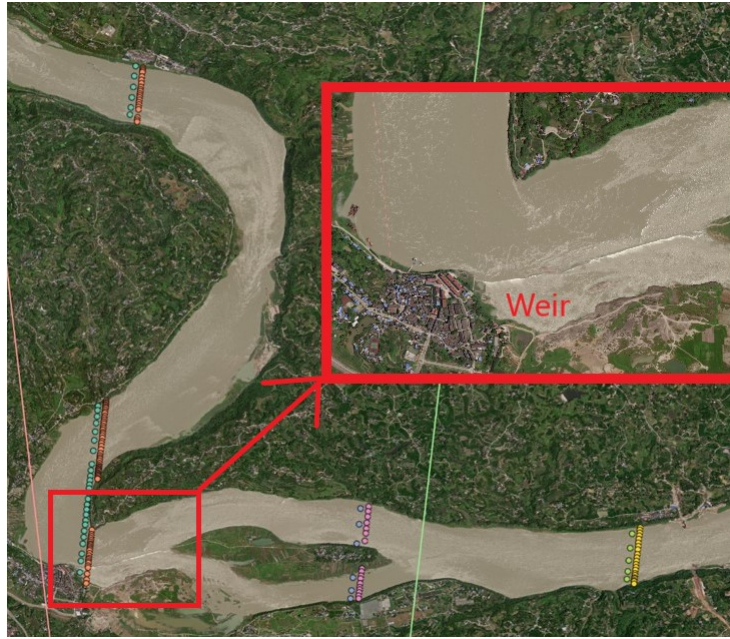


Figure 6.5: The weir near middle point 3

6.1.3 Comparison of the heights at two epochs

Table 6.3: The differences of the heights of two epochs

05.31.2019	C1	C2	C3	C4	C5
Strong beam (m)	219.30	217.90	217.94	215.78	214.12
27.08.2020	C1	C2	C3	C4	C5
Strong beam (m)	223.61	222.12	222.03	220.64	219.61
Diff (m)	-4.31	-4.21	-4.09	-4.85	-5.49

The results for each overlapping part at two epochs could also be compared. Table 6.3 shows the differences of overlapping areas on two different days. These differences display a kind of the definite difference that overall (at least for this study area) the water level on 29.08.2020 had an increase in the range of 4.09 m to 5.49 m compared to the water level on 31.05.2019. In order to validate the changes of water level, the correspondingly most suitable satellite images (Landsat-8) are selected for both epochs. Figure 6.6 is used to represent the day 31.05.2019 because there is no Landsat-8 image available on the exact same day.



Figure 6.6: The satellite image on 05.06.2020 (credit: Landsat-8)



Figure 6.7: The satellite imagery on 29.08.2020 (credit: Landsat-8)

From above pictures, in Figure 6.7 the water level is obviously higher than the water level in Figure 6.6. Because the river island in August got slightly flooded but in July it didn't get flooded. Therefore, the reasonable doubt is that the differences of heights between two epochs are resulted from the river's own water level fluctuations during the summer flood season.

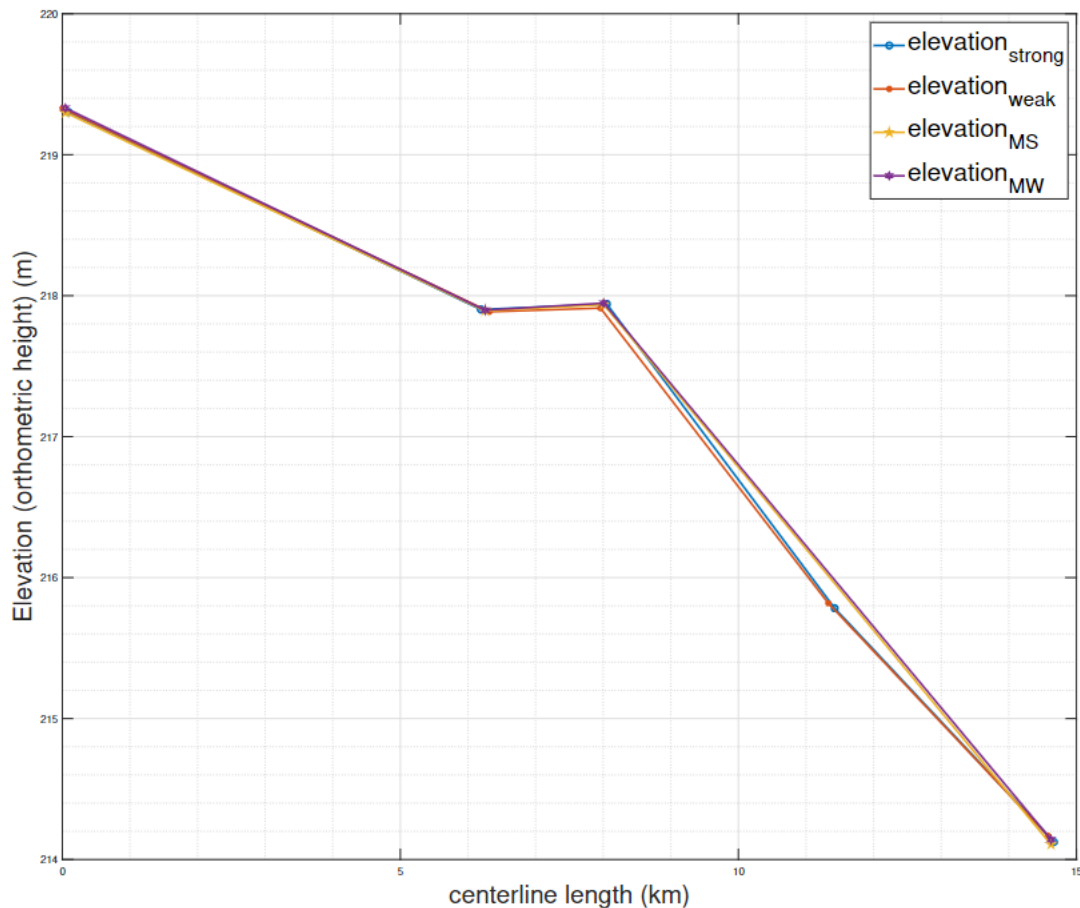


Figure 6.8: The calculated water levels of 4 different types of points on 31.05.2019

elevation_{strong}: the height of intersection calculated from strong beam

elevation_{weak}: the height of intersection calculated from weak beam

elevation_{MS}: the height of middle point calculated from strong beam

elevation_{MW}: the height of middle point calculated from weak beam

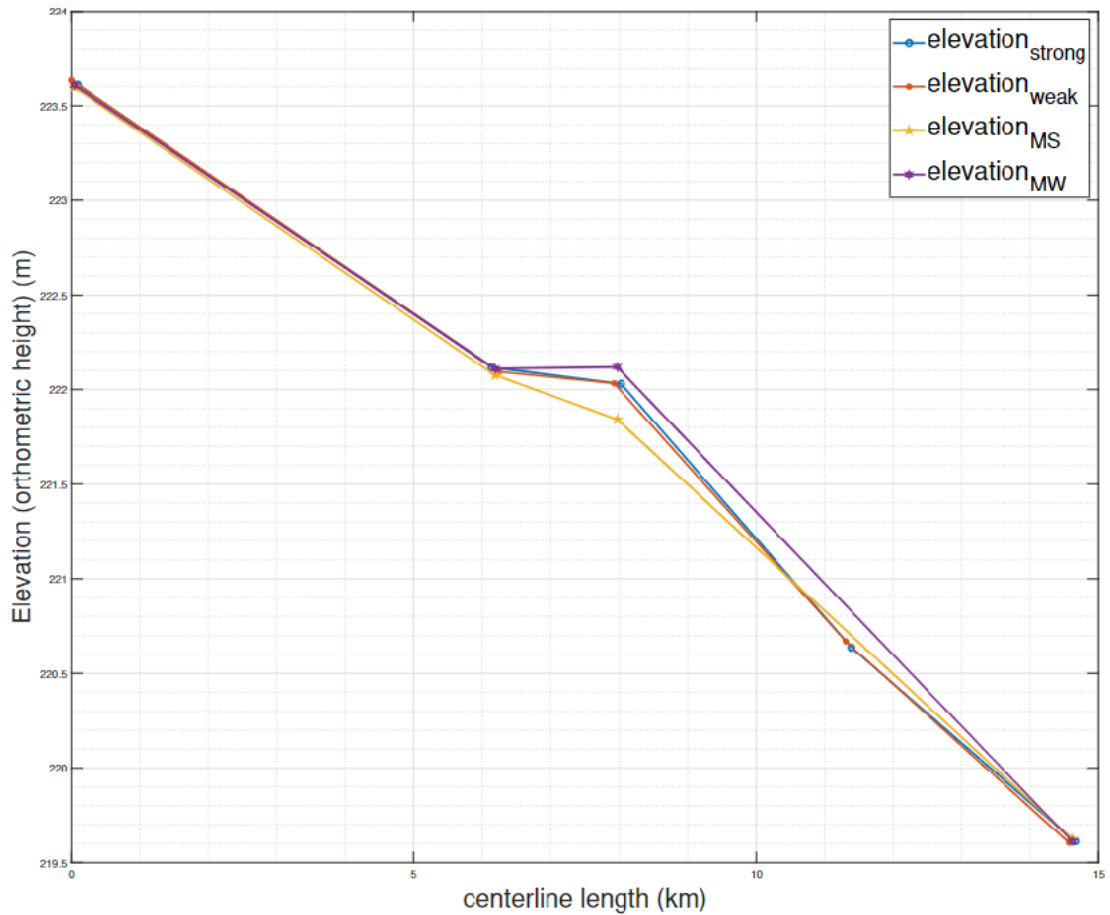


Figure 6.9: The calculated water levels of 4 different types of points on 27.08.2020

elevation_{strong}: the height of intersection calculated from strong beam

elevation_{weak}: the height of intersection calculated from weak beam

elevation_{MS}: the height of middle point calculated from strong beam

elevation_{MW}: the height of middle point calculated from weak beam

6.2 The heights derived from satellite track No.728

For the track ID 728, it has available data of the study area on 10.11.2020 and on 10.08.2021. The three satellite ground tracks (gt1, gt2, gt3) at two epochs had one track lateral displacement which can be seen from Figure 6.10.



Figure 6.10: Track ID728 on two epochs

6.2.1 The validation of the height of each intersection

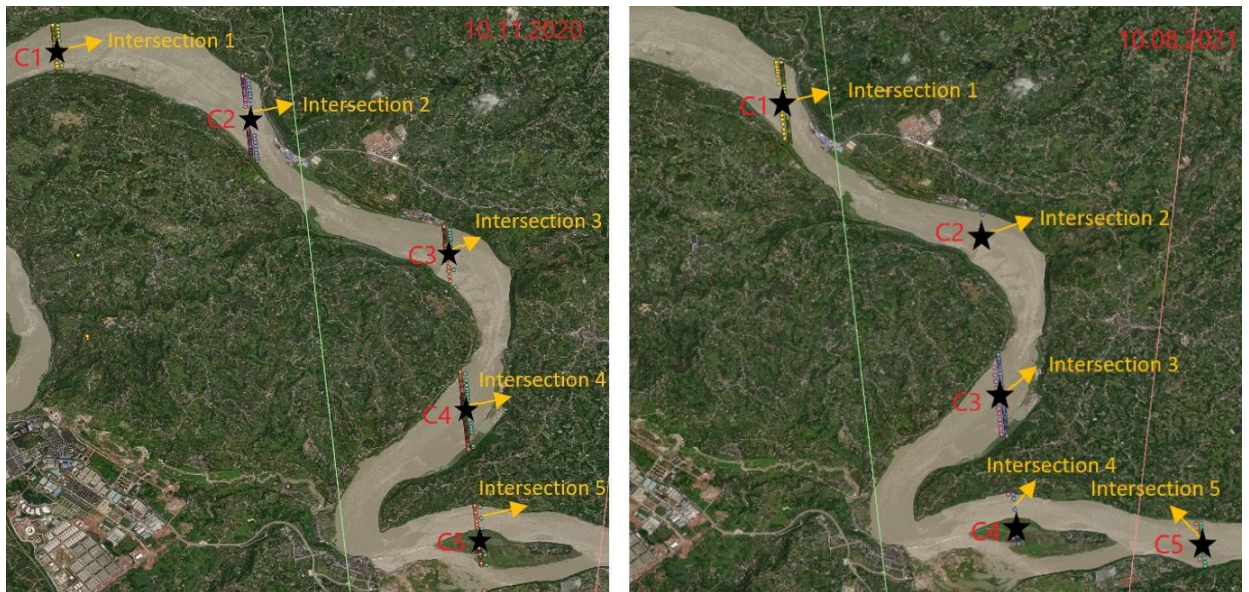


Figure 6.11: Track ID 728 Intersections

Table 6.4: The results of the heights derived from Track ID 728

10.11.2020	C1	C2	C3	C4	C5	RMSE
Strong beam (m)	221.18	219.84	219.18	218.32	216.88	
Weak beam (m)	221.17	219.87	218.91	218.40	216.75	
Diff (cm)	1	-3	27	-8	13	14
10.08.2021	C1	C2	C3	C4	C5	RMSE
Strong beam (m)	220.01	219.53	218.59	217.04	215.01	
Weak beam (m)	220.03	219.57	218.52	217.06	215.06	
Diff (cm)	-2	-4	7	-2	-5	5

From Table 6.4 it is obvious that there is a bigger difference of the heights between strong and weak beams for C3 on 10.11.2020 which is 27 cm. Nevertheless, for the corresponding same intersection C2 on 10.08.2021, the height difference of -4 cm is much smaller.

The reason of such change is the weir which can be seen from Figure 6.12. Because of the weir, when the water surface height is higher on 10.08.2021, the water may flood the weir and the weir cannot retain the water. On the contrary, when the water surface height is a bit lower on 10.11.2020, the weir emerges from the water and holds the water. This makes the height derived from weak beam smaller and

the difference between strong and weak beams on 10.11.2020 bigger.



Figure 6.12: A pair of track (10.11.2020) passed over the weir

6.2.2 The validation of the height of each middle point

Here comes the special case - River island, which makes it meaningless to calculate the water level on the middle point in that area. Owing to the satellite ground track intersects with the centerline of Yangtze River on the island, the height actually represents the elevation of the island rather than the water level. As the result, there is no point of projecting the satellite ground track onto the centerline of the river. Therefore, in this case, the height under this situation is omitted.

For the data on 10.08.2021 there are too few available data points around middle point 2 which can be seen from Figure 6.10, thus, the water level on M2 is not analysed on that day.

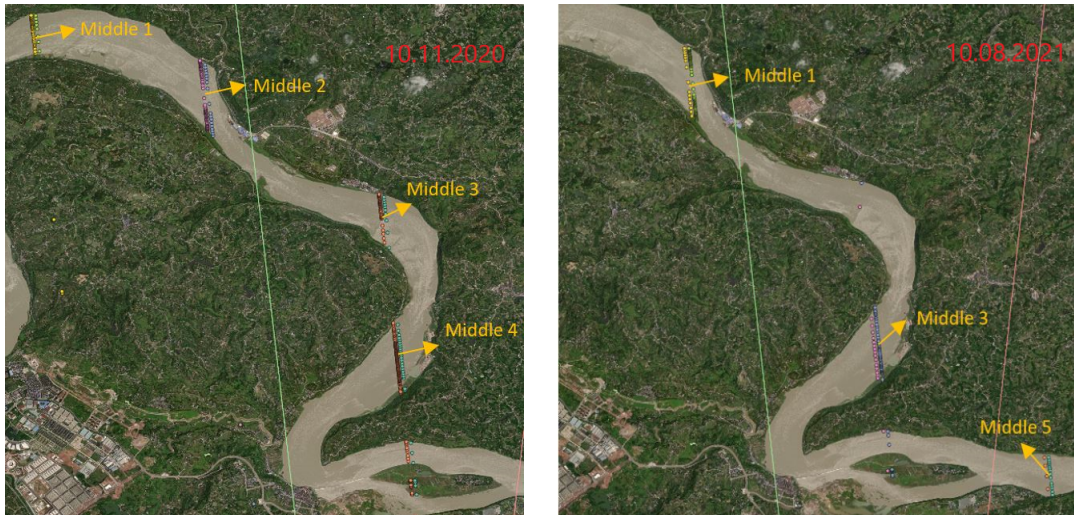


Figure 6.13: Track ID728 Middle points

Table 6.5: The results of the heights on Middle points

10.11.2020	M1	M2	M3	M4	RMSE
Strong beam (m)	221.16	219.82	219.39	218.34	
Weak beam (m)	221.14	219.86	219.04	218.38	
Diff (cm)	2	-4	35	-4	18
10.08.2021	M1		M3	M5	RMSE
Strong beam (m)	220.06		218.56	214.98	
Weak beam (m)	220.04		218.49	215.14	
Diff (cm)	2		7	-16	10

The reason for the big height difference (35 cm) of M3 on 10.11.2020 from Table 6.5 has been explained before.

6.2.3 The comparison of the heights at two epochs

Firstly, Table 6.4 shows clearly that on the same day the derived heights from strong and weak beams of the overlapping parts are quite similar except the part where the weir locates.

Secondly, the results at two epochs for each same part could be compared. Table 6.6 demonstrates the height differences between two different epochs from strong beams.

Table 6.6: The differences of the heights at two epochs

10.11.2020	C2	C3	C4	C5
Strong beam (m)	219.84	219.18	218.32	216.88
10.08.2021	C1	C2	C3	C4
Strong beam (m)	220.01	219.53	218.59	217.04
Diff (cm)	-17	-34	-28	-16

These differences show that the water level on 10.08.2021 is slightly higher than the water level on 10.11.2020, which can be validated from the correspondingly most suitable satellite images. Figure 6.14 is used to represent 10.11.2020 and Figure 6.15 is used for 10.08.2021.

From Figure 6.14 and Figure 6.15 it is clear that the area, which is marked out, got slightly flooded on 04.08.2021 compared to the same area on 12.11.2020. This means the water surface height was a bit higher on 10.08.2021, which is coincident with the calculated water level differences.



Figure 6.14: The satellite image on 12.11.2020 (credit: Landsat-8)



Figure 6.15: The satellite image on 04.08.2021 (credit: Landsat-8)

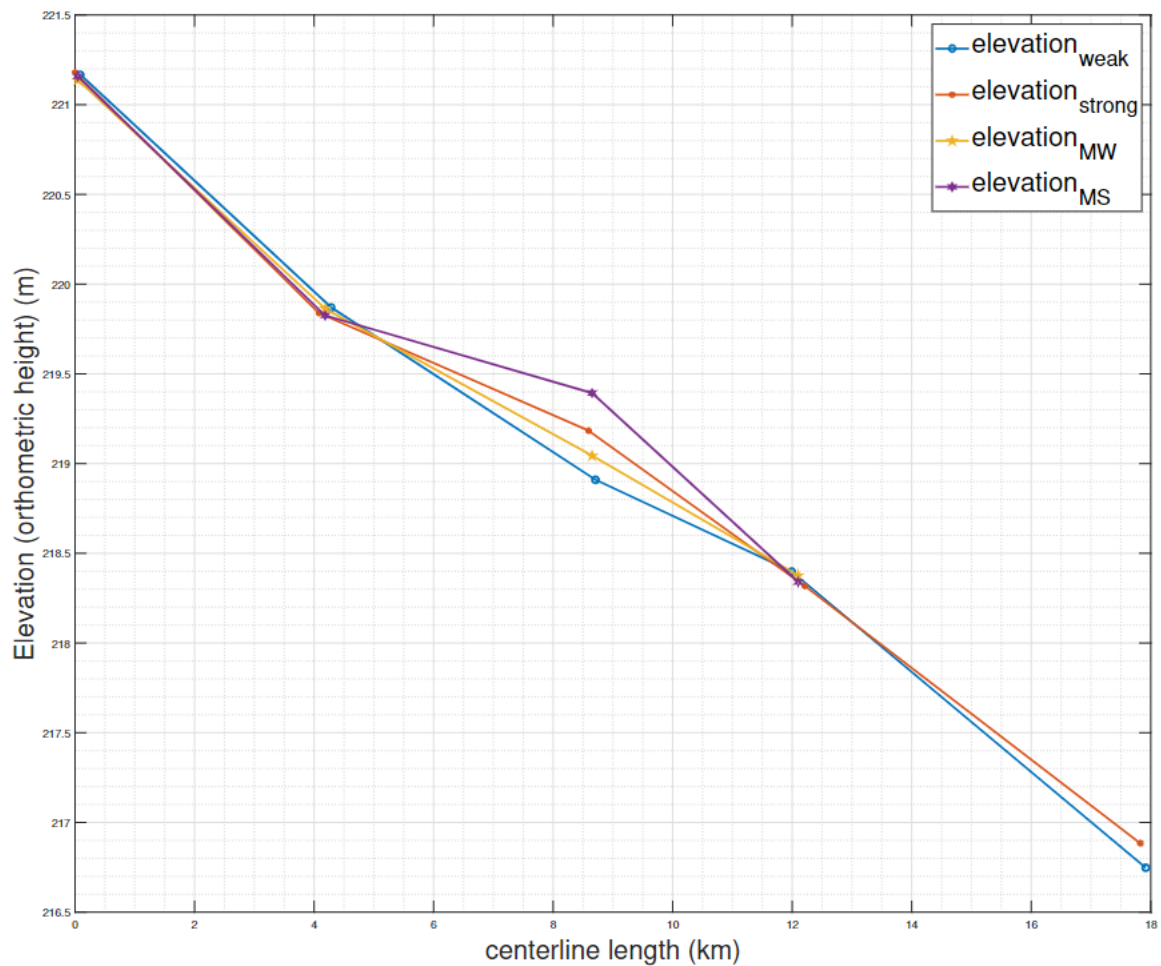


Figure 6.16: The calculated water levels of 4 different types of points on 10.11.2020

elevation_{strong}: the height of intersection calculated from strong beam

elevation_{weak}: the height of intersection calculated from weak beam

elevation_{MS}: the height of middle point calculated from strong beam

elevation_{MW}: the height of middle point calculated from weak beam

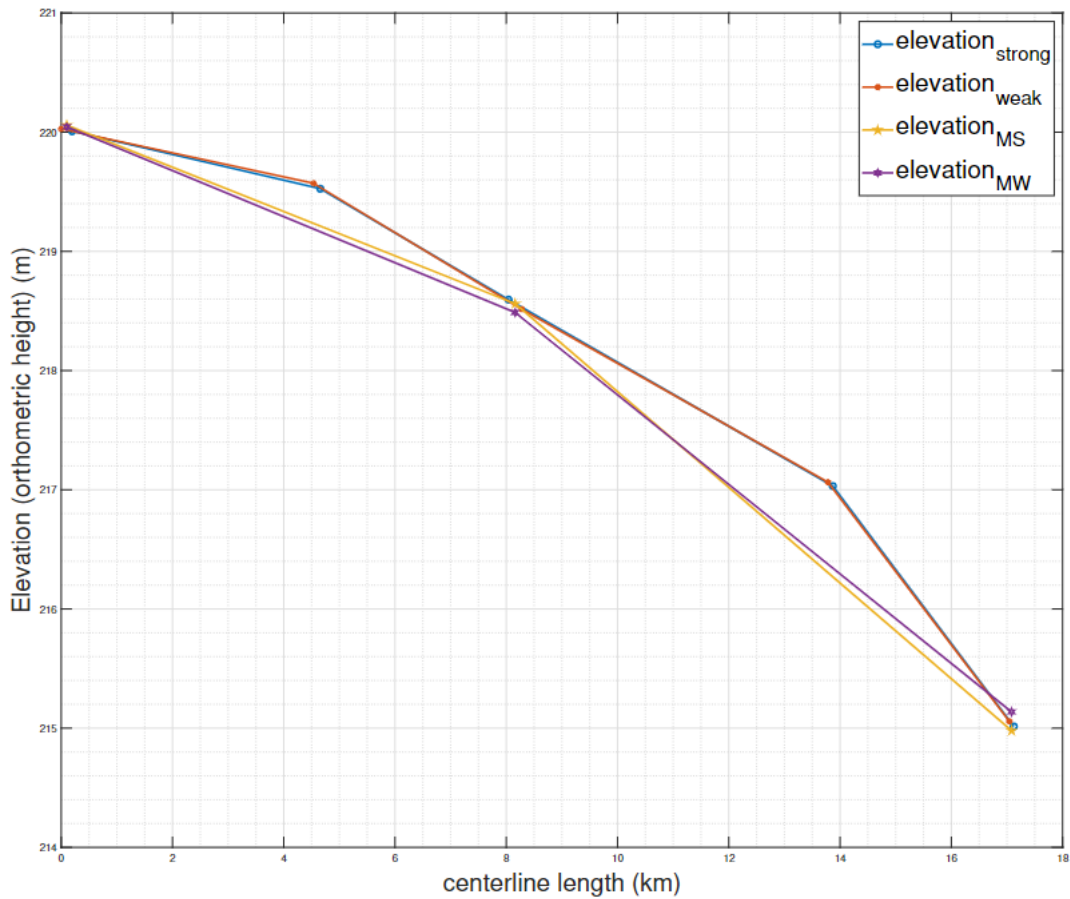


Figure 6.17: The calculated water levels of 4 different types of points on 10.08.2021

$elevation_{strong}$: the height of intersection calculated from strong beam

$elevation_{weak}$: the height of intersection calculated from weak beam

$elevation_{MS}$: the height of middle point calculated from strong beam

$elevation_{MW}$: the height of middle point calculated from weak beam

6.3 Slope of the reach

6.3.1 Results derived from satellite track No.964

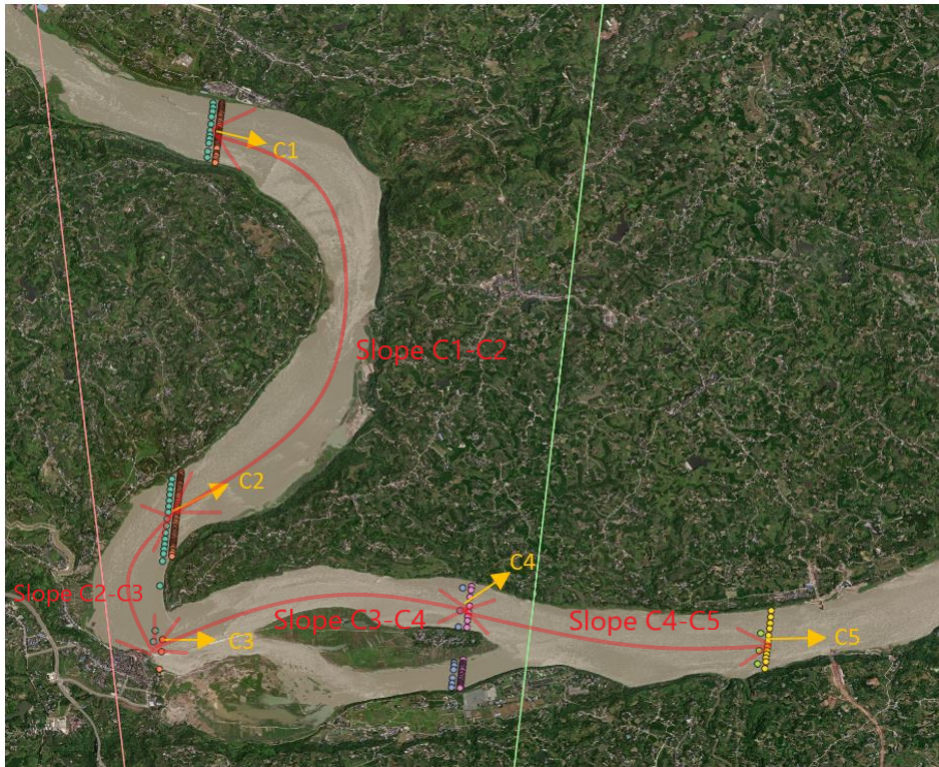


Figure 6.18: The slopes of the reach derived from track ID 964

Table 6.7: The differences of the results at two epochs

31.05.2019	Slope C1-C2 (cm/km)	Slope C2-C4 (cm/km)	Slope C4-C5 (cm/km)
Strong beam	23	40	51
Weak beam	23	41	51
Diff (cm/km)	0	-1	0
27.08.2020	Slope C1-C2 (cm/km)	Slope C2-C4 (cm/km)	Slope C4-C5 (cm/km)
Strong beam	25	28	31
Weak beam	25	28	33
Diff (cm/km)	0	0	-2

Firstly is the horizontal comparison between slopes. The length of each reach is different and the total length from C1 to C5 is more than 10 km, therefore the slope of each reach couldn't be constant.

Secondly comes the vertical comparison of the overlapping reaches at two epochs. The velocity of the river will change according to the seasons. At two different epochs the velocity of the river is different, thus the water level is different and in the end the calculated slope is different.

From the satellite image there is a small weir at the bend of the river. In August, the water level increased and flooded the weir, which means the weir could not retain the water at that time and lost its function. Therefore, the slope would be slightly flatter.

On the contrary, the water level in May was lower and the weir emerged from the water and would hold water at certain extent. Therefore, the slope would be slightly steeper.

6.3.2 Results derived from satellite track No. 728

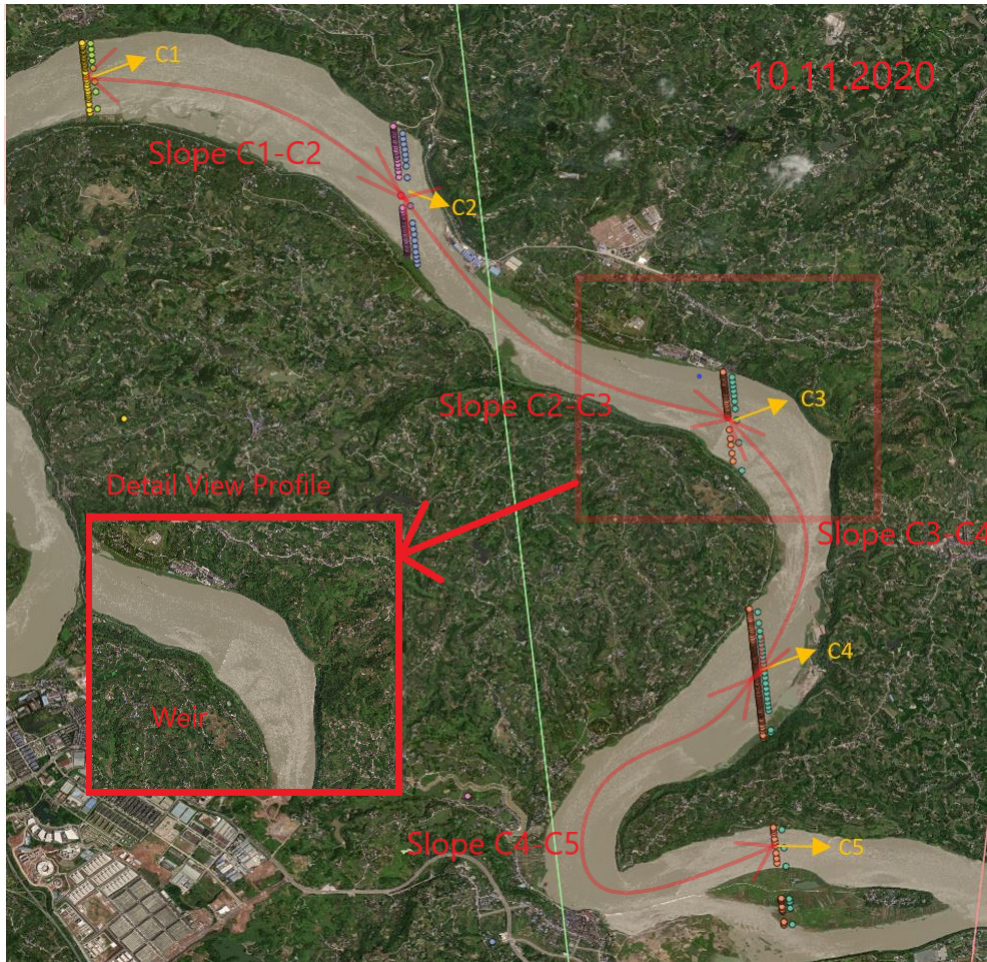


Figure 6.19: The slopes of the reach derived from track ID 728 on 10.11.2020

Table 6.8: The slopes of track ID 728 on 10.11.2020

10.11.2020	C1-C2	C2-C3	C3-C4	C4-C5	C2-C4
Strong beam (cm/km)	33	14	24	26	19
Weak beam (cm/km)	31	22	16	28	19
Diff (cm/km)	2	-8	8	-2	0

From Table 6.8 there exist big differences of the slope C2-C3 and slope C3-C4 between strong and weak beams on the same day. The reason behind might be the weir locating near C3 which can be seen from Figure 6.19. During the non-flooding season the water level is low and the weir would emerge from the river and retain the water. This would result in the bigger difference of water heights

between the upper and lower sides of the weir.

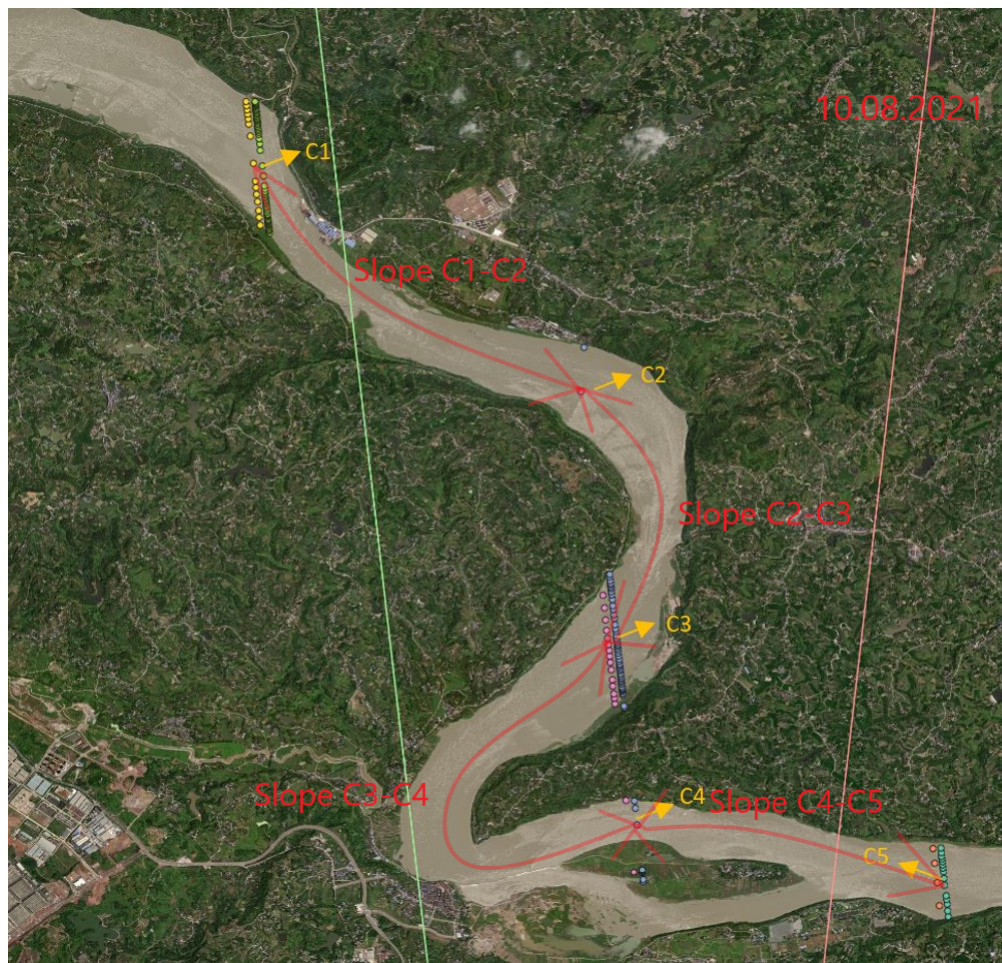


Figure 6.20: The slopes of the reach derived from track ID 728 on 10.08.2021

Table 6.9: The results of track ID 728 on 10.08.2021

10.08.2021	Slope C1-C2	Slope C2-C3	Slope C3-C4	Slope C4-C5
Strong beam (cm/km)	11	28	27	62
Weak beam (cm/km)	10	28	26	61
Diff (cm/km)	1	0	1	1

From Table 6.9 the differences of the slopes between strong and weak beams are quite small (maximal 1 cm) on 10.08.2021, which means the weir locating close to C2 cannot retain the water. This is because August is the flooding month of Yangtze River, therefore, the water will flood the weir which makes the weir lose its function.



Figure 6.21: The overlapping area of track ID 728 at two epochs

Table 6.10: The comparison of the results of track ID 728 at two epochs

10.11.2020	Slope C2-C3	Slope C3-C4	Slope C4-C5
Strong beam (cm/km)	14	24	26
10.08.2021	Slope C1-C2	Slope C2-C3	Slope C3-C4
Strong beam (cm/km)	11	28	27
Diff (cm/km)	3	-4	-1

From Table 6.10, the biggest difference of the slopes between two epochs is -4 cm/km, this means the overlapping reaches have quite similar results of slopes.

6.3.3 The comparison of the results between track No.964 and track No.728 in close areas



Figure 6.22: The overlapping areas

Table 6.11: The comparison between track ID 728 and track ID 964

Track ID 728 on 10.11.2020	Slope C3-C4	Slope C4-C5
Strong beam (cm/km)	24	26
Track ID 964 on 10.08.2021	Slope C1-C2	Slope C2-C4
Strong beam (cm/km)	25	28
Diff (cm/km)	-1	-2

From above Table 6.11, the biggest difference of the slopes between twp tracks is 2 cm/km, this means the overlapping reaches have quite similar results.

6.4 Slope between strong and weak beam in one pair

6.4.1 Results derived from satellite track No.964

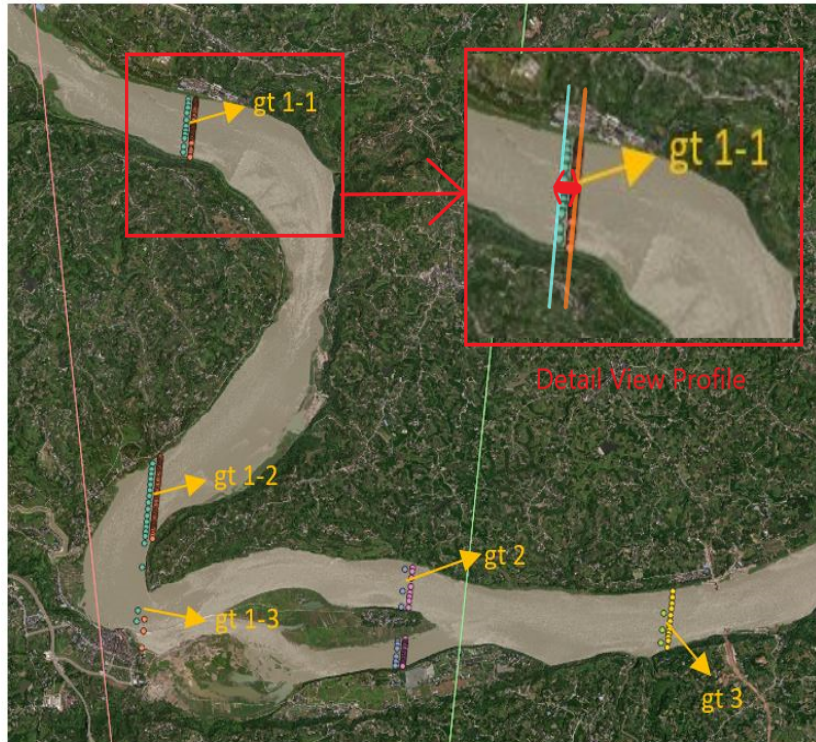


Figure 6.23: The slopes between strong and weak beam in one pair from track ID 964 on 31.05.2019

Table 6.12: The results of track ID 964 at two epochs

31.05.2019	gt1-1	gt1-2	gt1-3	gt2	gt3
Slope (cm/km)	-28	-12	28	-38	-50
27.08.2020	gt1-1	gt1-2	gt1-3	gt2	gt3
Slope (cm/km)	-28	-19	-4	-35	-8

From Table 6.12, comparing to the slope of the reach, the results of the slope between strong and weak beam within one pair have much bigger differences with the range from -50 cm/km to 28 cm/km. The reasons might be as follows:

Firstly is the error propagation. The heights measured at strong and weak beams within one pair already have error. According to the equation $slope = \frac{\Delta h}{d}$, when d is small (a little bit more than 90 m), the error of the calculated slope will be big. However, for the slope of the reach, d is several kilometers, thus the error of the

slope will be relatively small.

Secondly, there is a big difference of the slopes of gt 1-3 between two epochs. Moreover, on 31.05.2019 the value is 28 cm/km which is even positive. For this, the different measurement months are the reason behind. May is not the flooding season of Yangtze River so the water cannot flood the weir. Therefore, the weir would retain the water and the water level close to the weir would be higher. On the contrary, August is the flooding season, thus the water would flood the weir and the calculated slope would be negative. This can be seen from Figure 6.24.

Thirdly, the slopes of gt3 at two epochs have big difference which is probably resulted from the different satellite data densities of this area. On 31.05.2019, gt3 had more data points than on 27.08.2020 which can be seen from Figure 6.25. Therefore the result of slope gt3 is more reliable on 31.05.2019 than on 27.08,2020.



Figure 6.24: Track ID964 gt1-3 on 31.05.2019 and on 27.08.2020



Figure 6.25: The data points of gt3 on 31.05.2019 and on 27.08.2020

6.4.2 Results derived from satellite track No.728

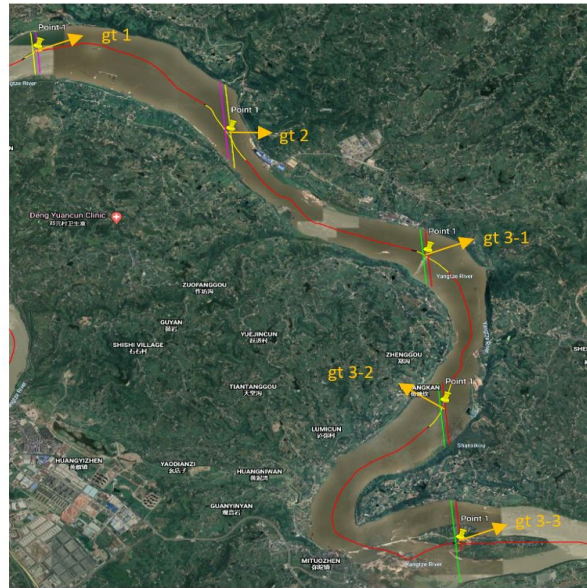


Figure 6.26: The slopes between strong and weak beam in one pair from Track ID728 on 10.11.2020

Table 6.13: The results of Track ID728 on 10.11.2020

10.11.2020	gt1	gt2	gt3-1	gt3-2	gt3-3
Slope (cm/km)	-14	16	-234	-37	-154

From Table 6.13 there exist three abnormal values (gt 2, gt 3-3 and gt 3-1). The reasons might be as follows:

First is the result of gt2 of 16 cm/km. From Figure 6.27 it can be seen that on 10.11.2020 gt2 even didn't have data points close to the centerline of the river. This means the heights of strong and weak beams couldn't represent the water level along the centerline of the river. Moreover, the rest satellite measurements had originally error. However, according to the error propagation, the error will be bigger when the distance between strong and weak beams in one pair is small.

Second is the result of gt3-3 of -154 cm/km. It is obvious that the intersection points between gt 3-3 and the centerline of the river are on the river island. Therefore the calculated results represented the island elevation instead of the water level.

Third is the result of gt 3-1 of -234 cm/km, which is bigger than the others. The reason behind is the weir which can be seen from Figure 6.28. The weir has the function of holding the water, therefore, the difference between the heights of strong and weak beams would be a big bias.



Figure 6.27: Track ID728 gt2 on 10.11.2020

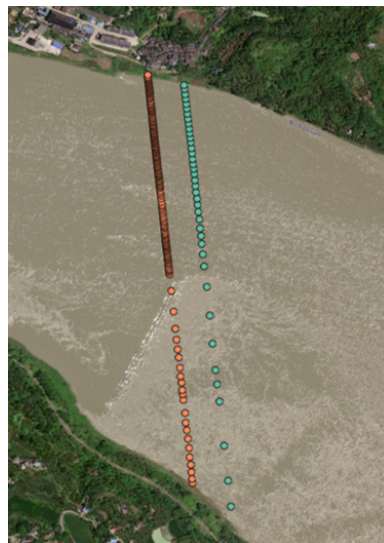


Figure 6.28: Track ID728 gt3-1 on 10.11.2020

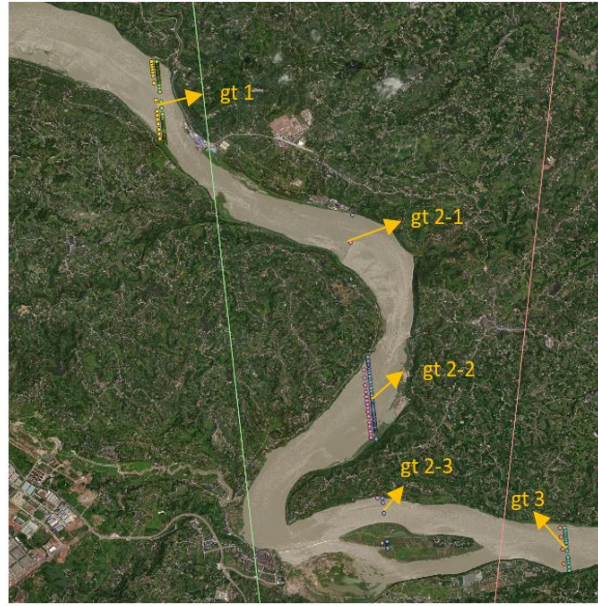


Figure 6.29: The slopes between strong and weak beam in one pair from Track ID728 on 10.08.2021

Table 6.14: The results of Track ID728 on 10.11.2020

10.08.2021	gt1	gt2-1	gt2-2	gt2-3	gt3
Slope (cm/km)	-10	-38	-33	-36	-53

From Table 6.13 and 6.14 ,the conclusion that the slope between strong and weak beams within one pair is less reliable and more likely to have unreasonable values caused by the local conditions like the weir. Because the differences of the slope of the reach are only several centimeter per kilometer, on the contrary, the differences of this type of slope could be tens of centimeters per kilometer. Moreover, the distance between two beams is relatively small. Therefore, even a relatively small error of the height could also result in the big error of slope due to the error propagation. In addition, the bias between strong and weak beams should also be considered, which makes the slope between strong and weak beam in one pair even more inaccurate.

6.5 Slope along the river in one beam

6.5.1 Results derived from satellite track No. 964

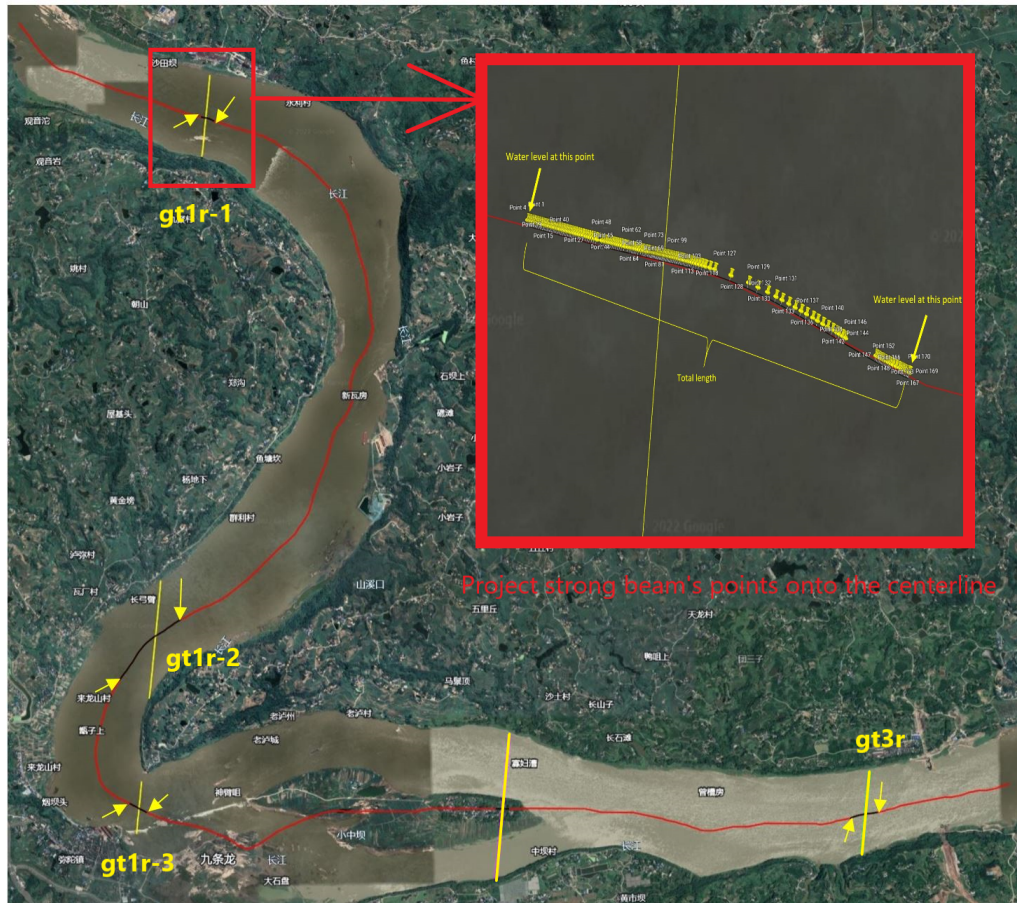


Figure 6.30: Track ID 964 *strong beams* projection

Table 6.15: The results of Track ID 964 at two epochs

31.05.2019	gt1r	gt1r-2	gt1r-3	gt3r
Slope (cm/km)	13	1	37	5
27.08.2020	gt1r	gt1r-2	gt1r-3	gt3r
Slope (cm/km)	47	24	73	26

From Table 6.15 there is an abnormal value of slope gt1r-3, comparing to the other calculated values if man observes the table horizontally. The reason of the larger difference in water level along the track is probably the weir, which can be seen from Figure 6.30. Since the weir which has the function of retaining the water, the water level close to the weir will be much higher. Moreover, gt1r-3 is close to be perpendicular to the centerline of the river. Therefore, this kind of slope could

also be considered as cross section slope which is influenced by the curvature and velocity of the stream.

In this case, gt1r-2 is very inclined to the centerline of the river, comparing to the other three satellite ground tracks. This means, after projection, the projected lengths of the other three tracks are very small, therefore, even a small height difference can cause large slope. Moreover, the small height difference could be resulted from the satellite measurement error rather than the slope.

6.5.2 Results derived from satellite track No.728 on 10.11.2020

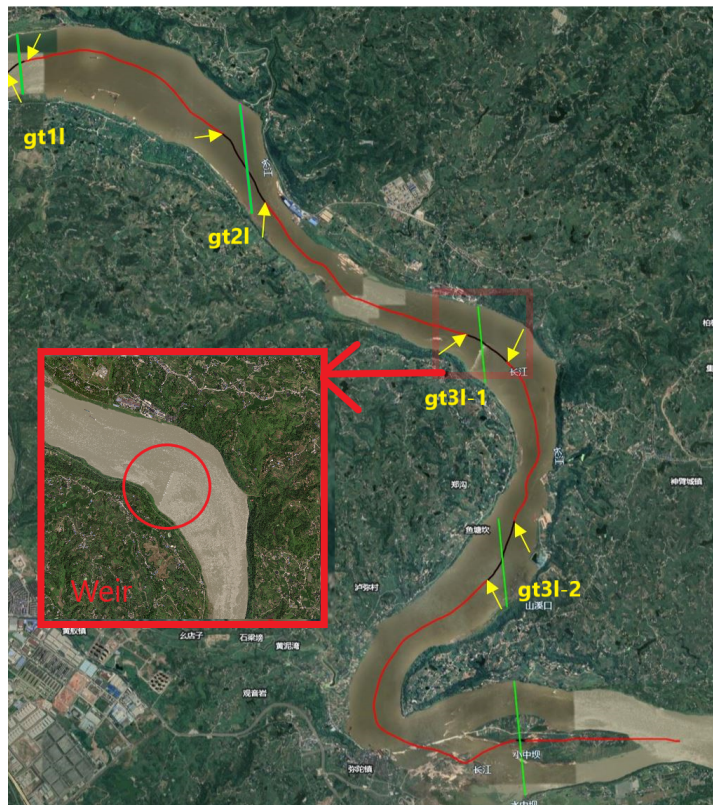


Figure 6.31: Track ID 728 *strong beam* projection on 10.11.2020

Table 6.16: The results of Track ID 728 on 10.11.2020

10.11.2020	gt11	gt21	gt31-1	gt31-2
Slope (cm/km)	23	5	41	3

From Table 6.16 the calculated result of slope gt31-1 is 41 cm/km which is bigger than the others. The reason behind is the weir, which is shown in Figure 6.31. Moreover, the result of gt11 is 23 cm/km which is also big. This is because gt11

is close to be perpendicular to the centerline of the river, therefore, the projected length of this track is very small. In this situation, even a small height difference can lead to a large slope.

6.5.3 Results derived from satellite track No.728 on 10.08.2021

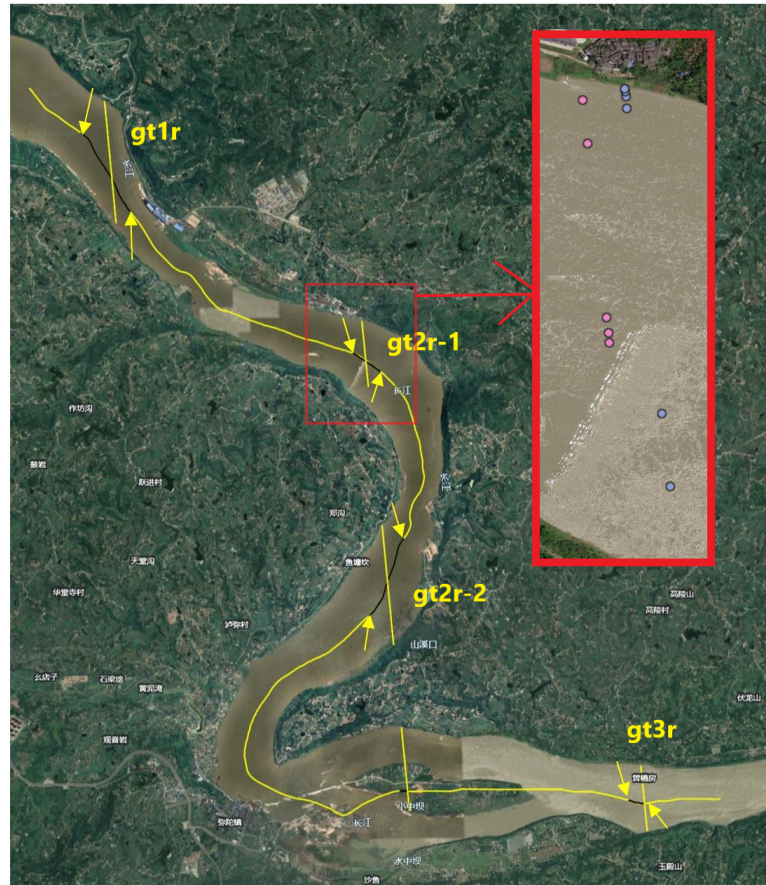


Figure 6.32: Track ID 728 *strong beam* projection on 10.08.2021

Table 6.17: The results of Track ID 728 on 10.08.2021

10.08.2021	gt1r	gt2r-1	gt2r-2	gt3r
Slope (cm/km)	16	502	11	11

From Table 6.17 there also exists an extreme value of slope gt2r-1, which is correspondingly also resulted from the weir. Moreover, it can be seen from Figure 6.32 that the available data points of gt2r-1 is obviously too few and most of the data points locate close to the bank of the river rather than the centerline. This makes the calculated slope more inaccurate.

6.6 Slope of the river cross section

6.6.1 Results derived from satellite track No.964 on 31.05.2019

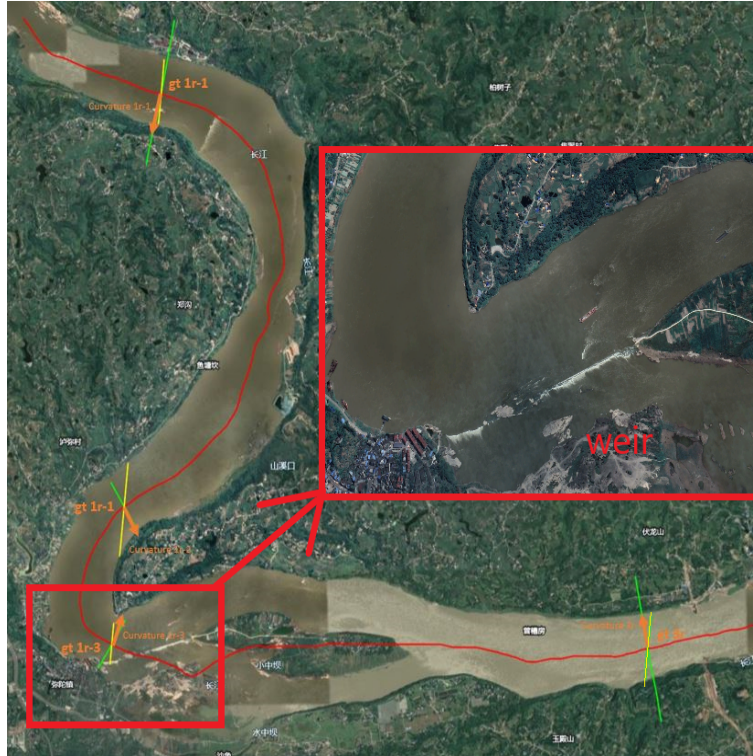


Figure 6.33: The norms of the centerline of the river and the satellite ground tracks on 31.05.2019

Table 6.18: The results of Track ID 964 on 31.05.2019

31.05.2019	gt1r-1	gt1r-2	gt1r-3	gt3r
curvature (km^{-1})	0.14	0.90	0.48	0.07
slope (cm/km)	2.2	2.5	22.4	1.7

From Table 6.18 the section gt3r has the curvature value of 0.07 km^{-1} , which means in this segment the river is relatively straight. Hence, for the straight stream shape the cross section slope is less obvious than the other segments with larger curvatures. Moreover, comparing to gt1r-1 and gt1r-2, even though the curvature value of gt1r-3 agrees with the other two in the same order, the value of the slope is bigger. From my point of view this is because of the weir. From Figure 6.33 there is a weir in the section gt1r-3 which influences the water surface height.

6.6.2 Results derived from satellite track No. 964 on 27.08.2020

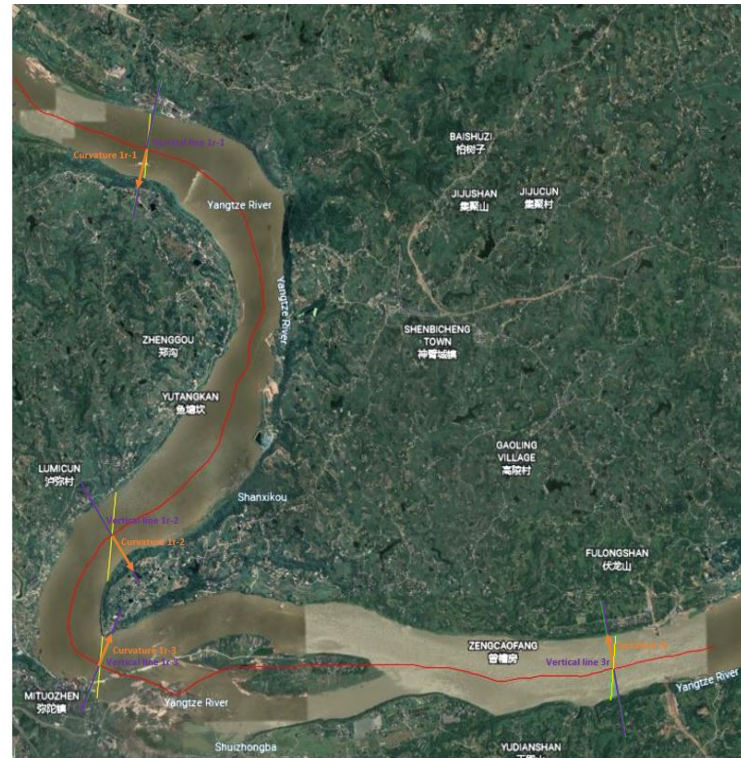


Figure 6.34: The *norms* of the *centerline* of the river and the *satellite ground tracks* on 27.08.2020

Table 6.19: The results of Track ID 964 on 27.08.2020

27.08.2020	gt1r-1	gt1r-2	gt1r-3	gt3r
curvature (km^{-1})	0.16	0.82	0.48	0.06
slope (cm/km)	7.4	23.3	23.6	9.7

From Table 6.19 the calculated curvature values of gt1r-1 and gt3r are correspondingly 0.16 km^{-1} and 0.06 km^{-1} , which are coincident with the values in Table 6.18. However, the slopes of the river cross section are bigger in August than in May because of the velocity of the stream. May is the non-flooding season so the velocity of the river is smaller. However, August is the flooding season so the velocity is bigger.

Moreover Table 6.19 shows a clear correlation between curvature and slope, but Table 6.18 doesn't. In Table 6.18 when the curvature is relatively big, the slope is still small which could be considered as no slope. For example, the curvature value of gt1r-2 is 0.90 km^{-1} but the slope is only 2.5 cm/km . The reason is the

velocity of the river is small in May so the centrifugal force is small.

6.6.3 Results derived from satellite track No. 728 on 10.11.2020



Figure 6.35: The norms of the centerline of the river and the satellite ground tracks on 10.11.2020

Table 6.20: The results of Track ID 728 on 10.11.2020

10.11.2020	gt11	gt21	gt31-1	gt31-2
curvature (km^{-1})	0.35	0.05	0.50	0.33
slope (cm/km)	7.7	10.4	22.6	5.5

From Table 6.20 it can be seen that in the segment of gt21 the curvature value is 0.05 km^{-1} , which means the stream shape is straight. However, the calculated

cross section slope value is 10.4 cm/km, which is relatively big. On the contrary, the curvature value of gt3l-2 is 0.33 km^{-1} , however, the slope value is 5.5 cm/km. This abnormal result reveals one major drawback of this method to calculate the river cross section slope.

For example, in this case, the satellite ground track gt2l is inclined to the centerline of the river. In this situation it is not reasonable to project the data points which are inclined to the centerline to the norm of the centerline. Because this slope is actually not the exact cross section slope. It is caused by the height difference along the river instead of the river cross section.

Moreover, gt3l-1 has a much bigger slope than that of gt1l, but the difference between the curvature values of gt1l and gt3l-1 is not that much. The reason behind might be the weir, which can be seen from Figure 6.35.

6.6.4 Results derived from satellite track No. 728 on 10.08.2021

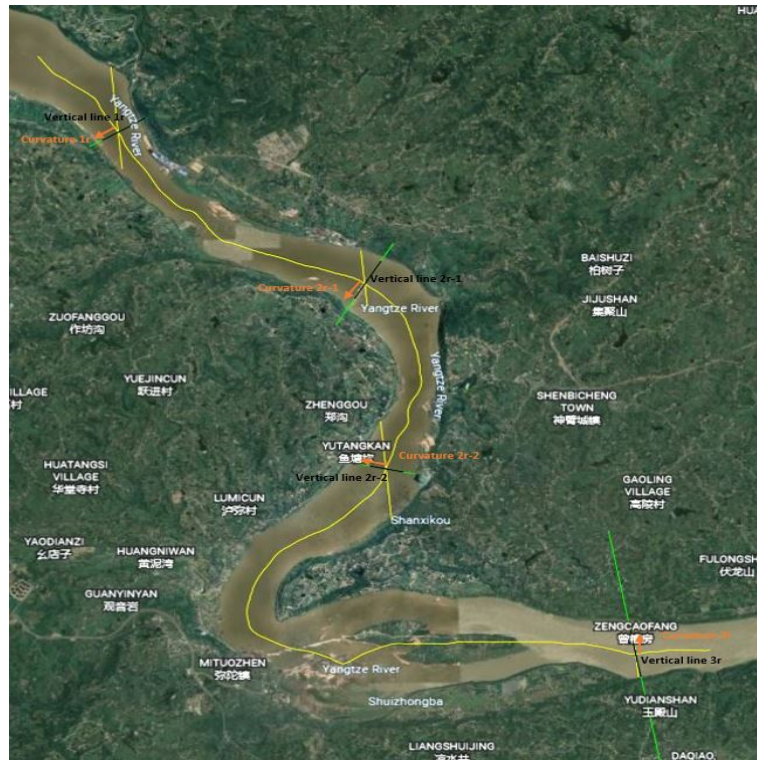


Figure 6.36: The *norms* of the *centerline* of the river and the *satellite ground tracks* on 10.08.2021

Table 6.21: The results of Track ID 728 on 10.08.2021

10.08.2021	gt1r	gt2r-1	gt2r-2	gt3r
curvature (km^{-1})	0.01	0.52	0.32	0.27
slope (cm/km)	34.8	48.0	27.9	3.3

From Table 6.21 the obtained curvature value in gt1r is 0.01 km^{-1} , therefore, we can consider this segment is a straight reach. In reality there should be no slope of the river cross section, however, we get a very large slope of 34.8 cm/km. The reason for this large slope value is already discussed before, which satellite track is too inclined to the centerline of the river.

The segments gt2r-2 and gt3r have similar curvature values, however, the cross section slopes are much different. This is because gt2r-2 is very inclined to the centerline, which means the slope of 27.9 cm/km cannot represent the cross section slope. On the contrary, gt3r is relatively perpendicular to the centerline of the river.

6.6.5 The comparison of the results of track No.728 at two epochs

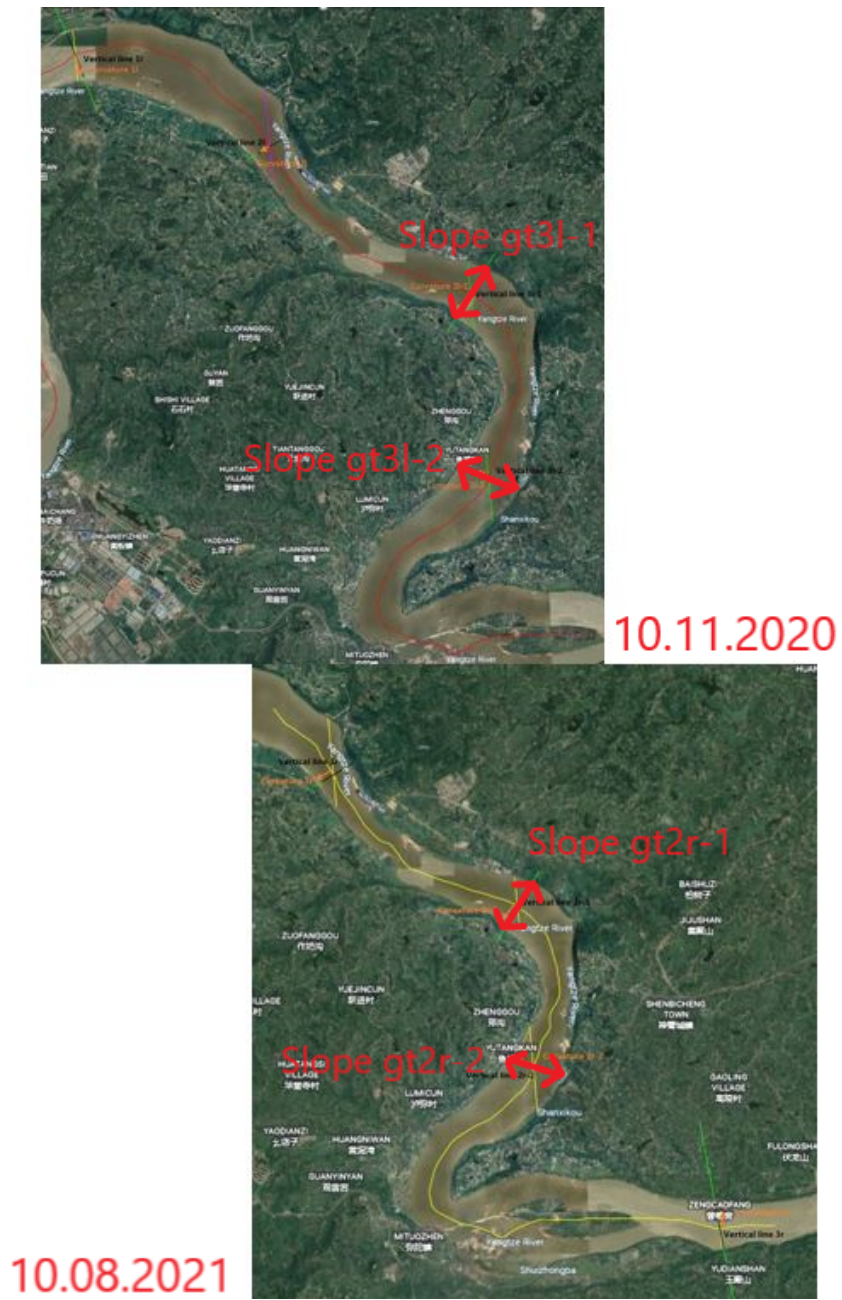


Figure 6.37: Track ID 728 at two epochs

Table 6.22: The results comparison of Track ID 728 at two epochs

10.11.2020	gt3l-1	gt3l-2
curvature (km^{-1})	0.50	0.33
slope (cm/km)	22.6	5.5
10.08.2021	gt2r-1	gt2r-2
curvature (km^{-1})	0.52	0.32
slope (cm/km)	48.0	27.9

In Table 6.22, gt3l-1 on 10.11.2020 and gt2r-1 on 10.08.2021 have overlapping areas. And gt3l-2 on 10.11.2020 and gt2r-2 on 10.08.2021 also have overlapping areas.

From the table above we could see that in overlapping areas, the differences between the calculated curvature values are small but the differences of the river cross section slopes are large. This is because the centrifugal force is determined not only by the curvature but also by the velocity of the stream. The higher the stream velocity is, the larger the river cross section slope could be. August is the flooding season of the river, therefore, the river flows much faster than the river in November. As the result, the slopes in August are larger than those in November.

Chapter 7

Results and validations of downstream of the Three Gorges Dam

7.1 Results of the calculated heights



Figure 7.1: The intersections of Track ID 95 on 04.04.2019

From Table 7.1 and Table 7.2 it is clear that the height differences between two neighbouring intersections.

Comparing to the previous study case in Chapter 6, the stream in this area flows much more gently. The reason behind is different topographies. In Chapter 6, the mountainous area leads to much more obvious changes in water level. However,

Table 7.1: The results of orthometric heights derived from Track ID 95

04.04.2019	Intersection1	Intersection2	Intersection3	RMS (cm)
Strong beam (m)	62.73	62.76	62.62	
Weak beam (m)	62.81	62.73	62.67	
Diff (cm)	-8	4	-5	5.7

*Figure 7.2: The intersections of Track ID 743 on 11.11.2020**Table 7.2: The results of orthometric heights derived from Track ID 743*

11.11.2020	Intersection1	Intersection2	Intersection3	RMS (cm)
Strong beam (m)	63.28	63.20	63.11	
Weak beam (m)	63.33	63.21	63.13	
Diff (cm)	-5	-1	-2	2.8

in this case, the study area locates in the downstream of the Three Gorges Dam. It is known that river velocity in the downstream of dam could be quite slow when the dam is not released.

7.2 Slope of the reach

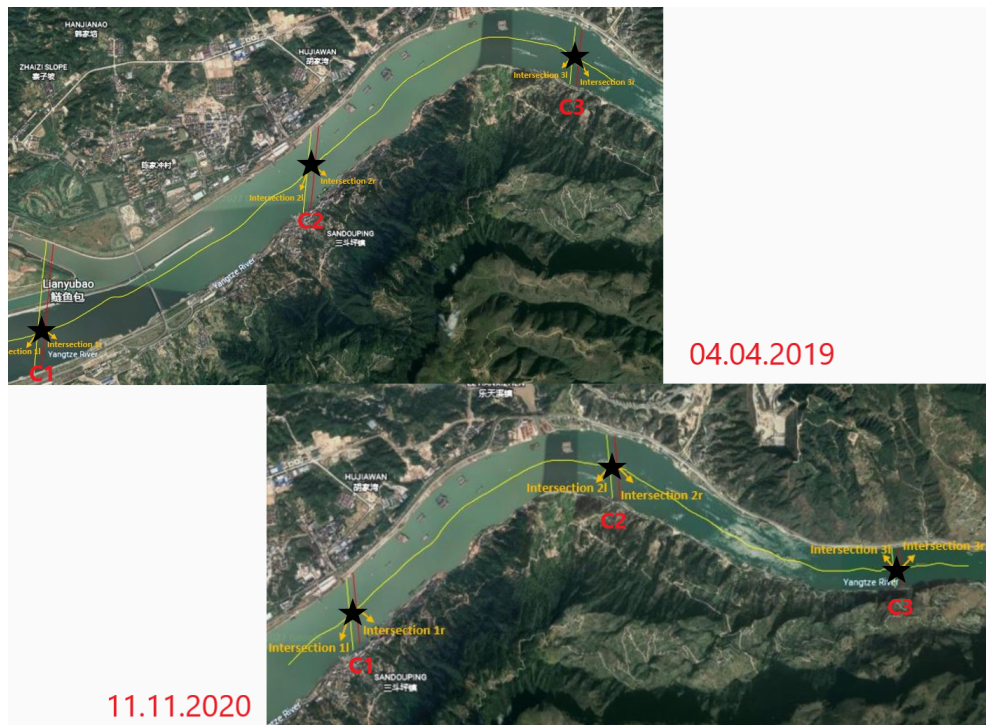


Figure 7.3: The overlapping area of satellite ground tracks

Table 7.3: Slopes of the reach derived from Track ID 95

04.04.2019	Slope C1-C2	Slope C2-C3
Strong beam (cm/km)	0	4
Weak beam (cm/km)	2	1
Diff (cm/km)	2	-3

From Table 7.3 and Table 7.4, it is obvious that comparing to the first study area, the slopes in this area are very small. It can be seen that the calculated results of the first and second study areas are one order of magnitude different. The reason behind is the dam and the topography of the area. The dam serves the primary purpose of retaining water and as a result the downstream after the dam is more like a peaceful flow than a raging one. Besides, the Three Gorges Dam situates

Table 7.4: Slopes of the reach derived from Track ID 743

11.11.2020	Slope C1-C2	Slope C2-C3
Strong beam (cm/km)	2	2
Weak beam (cm/km)	3	2
Diff (cm/km)	1	0

quite close to the Jiangnan Plain in Hubei Province, which is the confluence of the Yangtze and Han rivers.

For the slope between strong and weak beam in one pair and the slope along the river in one beam, considering the small values the slopes of the reach, these kinds of slopes can be negligible.

7.3 Slope of the river cross section



Figure 7.4: The norms of the centerline of the river on 04.04.2019

Table 7.5: The results of Track ID 95 on 04.04.2019

04.04.2019	Slope gt1r	Slope gt2r	Slope gt3r
curvature (km^{-1})	0.17	0.14	0.05
slope (cm/km)	0.10	3.74	1.24



Figure 7.5: The norms of the centerline of the river on 11.11.2020

Table 7.6: The results of Track ID 743 on 11.11.2020

11.11.2020	Slope gt11	Slope gt21	Slope gt31
curvature (km^{-1})	0.11	0.51	0.13
slope (cm/km)	1.54	4.79	7.94

In this study area the stream velocity is relatively small because of the retaining function of the dam. Hence, there is no strong relation between the calculated cross section slopes and the velocity of the river. The relation between the curvature of the river and the cross section slope would be more obvious. However, from Table 7.5 and Table 7.6, it can be seen that even when the curvature is smaller than the others, the derived slope could still be bigger. The reason behind is probably the water surface height measurement error. In this case, the river is narrow, therefore, the height difference of the cross section could be less than 1 cm. And this height difference might not be because of the cross section slope but the water surface height measurement error or the water waves.

7.4 Special case - the satellite ground tracks cross the dam



Figure 7.6: Track ID 743 on 15.08.2019

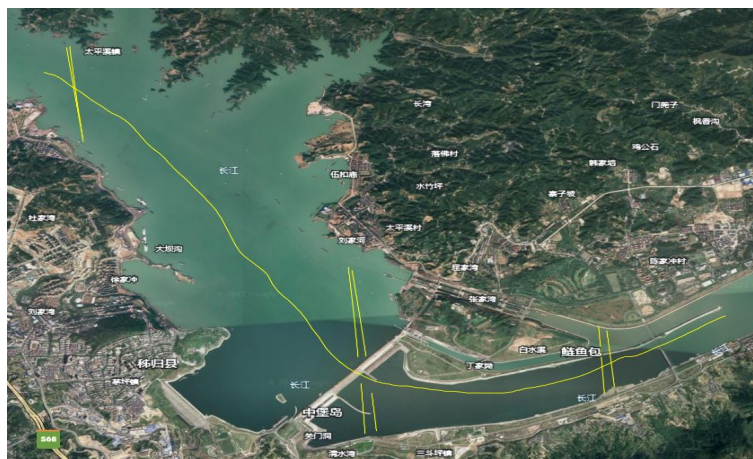


Figure 7.7: Track ID 743

In this case it can be seen from Google Earth that the satellite ground track passed the dam at this epoch. The reservoir held behind the dam also affects the topography of the river. The sawtooth flow pattern is caused by releases followed by no releases. Water releases from a reservoir including that exiting a turbine usually contain very little suspended sediment, and this, in turn, can lead to scouring of river beds and loss of riverbanks.

From Figure 7.7 the middle pair of the satellite ground track is split into two parts (upstream and downstream of the dam).

Table 7.7: The results of heights derived from Track ID 743

15.08.2019	Intersection1	Before dam 2	After dam 2	Intersection3
Strong beam (m)	144.72	144.79	64.68	64.36
Weak beam (m)	144.82	144.81	64.72	64.41
Diff (cm)	-10	-2	-4	-5

From Table 7.7 the height difference between upstream and downstream of the dam is about 80 m, which is within the maximal height difference of about 120 m. Moreover, from the derived height of each intersection point, it is obvious that the water surface height is relatively stable in upstream of the dam. This is because the Three Gorges Dam makes the upstream reservoir more like a peaceful lake and at the same time gives the downstream long periods of very stable flow conditions.

Chapter 8

Summary and conclusion

As a lack of ground gauge stations, the satellite altimetry technology is an effective way to globally observe the water surface of the earth. The application of satellite altimeter over inland water bodies has been explored and proven by many researches. Compared to radar altimetry, ICESat-2 laser altimetry provides a higher along-track spatial-resolution sampling. In this thesis, we studied large areas of Yangtze River in China using ICESat-2 to calculate four different types of slopes:

- Slope of the reach
- Slope between strong and weak beam in one pair
- Slope along the river in one beam
- Slope of the river cross section

From the experiments of the two cases, we have investigated the following conclusions:

- With the help of satellite data and SWORD dataset, we can get the positions of the centerline of Yangtze River and extract the river surface heights within the search radius.
- The slopes of the river are strongly influenced by seasons. During flooding and non-flooding seasons the slopes can vary a lot.
- There may be some complicated topographies in one reach. The weir, the river island and other possible elements will influence the water level significantly. Therefore, it is necessary to combine the calculated results with satellite images of the river, in order to recognise the influencing factors.

- Sometimes satellite measurements cannot provide sufficient data which are needed for calculating river height. Hence, it is important to adjust the data according to the particular case.

The ICESat-2 laser altimetry data has been shown to be able to monitor the inland surface water level and derive different types of slopes. However, the data is limited by many factors (e.g. topographies of the river and the pointing direction of laser beams) and sometimes data points could locate on the river island or the dam or close to the river bank instead of around the centerline. In addition, the temporal resolution of ICESat-2 is 91 days, thus, there is a high probability that events cannot be recorded. To solve this issue, it is necessary to use different satellite ground tracks and compare the water levels in overlapping areas.

Moreover, in order to obtain a relatively reliable results of slopes, it is important to combine the images of the river and the images of data points with the results and find out proper reasons for the abnormal or extreme values. Depending on the concrete case, not every type of slopes could be precisely calculated. Therefore, we should discriminate the situations and decide which type of slopes could be relatively precisely calculated.

References

- George H Allen and Tamlin M Pavelsky. Global extent of rivers and streams. *Science*, 361(6402):585–588, 2018. doi: 10.1126/science.aat0636.
- Morris Christopher G. Cleveland, Cutler J. *Handbook of Energy:Chronologies, Top Ten Lists, and Word Clouds*. Elsevier Science, 2013.
- Michael Jasinski, Jeremy Stoll, David Hancock, John Robbins, Jyothi Nattala, James Morison, Benjamin Jones, Michael Ondrusek, Tamlin Pavelsky, and Christopher Parrish. Algorithm theoretical basis document (atbd) for along track inland surface water data, release 004. 2021.
- Carabajal C. C. Saba J.L. Reese A. R. Holland S. T. Palm S.P. et al. McGarry, J. F. Icesat-2/atlas onboard flight science receiver algorithms: Purpose, process, and performance. *Earth and Space Science*, 2020.
- Thomas A Neumann, Anthony J Martino, Thorsten Markus, Sungkoo Bae, Megan R Bock, Anita C Brenner, Kelly M Brunt, John Cavanaugh, Stanley T Fernandes, David W Hancock, et al. The ice, cloud, and land elevation satellite–2 mission: A global geolocated photon product derived from the advanced topographic laser altimeter system. *Remote Sensing of Environment*, 233:111325, 2019. doi: 10.1016/j.rse.2019.111325.
- Zhiyu Zhang, Xinyuan Liu, Yue Ma, Nan Xu, Wenhao Zhang, and Song Li. Signal photon extraction method for weak beam data of icesat-2 using information provided by strong beam data in mountainous areas. *Remote Sensing*, 13(5): 863, 2021. doi: 10.3390/rs13050863.